Multi-omics analysis reveals discordant proteome and transcriptome responses in larval guts of *Frankliniella occidentalis* infected with an orthotospovirus

Jinlong Han[1] and Dorith Rotenberg[1*]

[1]North Carolina State University, Department of Entomology and Plant Pathology, Raleigh, North Carolina, 27695, U.S.A

Current address of J. Han: Department of Agricultural Biology, Colorado State University, Fort Collins, CO 80523, USA

[*] Correspondence: Dorith Rotenberg, Email: drotenb@ncsu.edu

Abstract. The western flower thrips, *Frankliniella occidentalis*, is the principal thrips vector of *Orthotospovirus tomatomaculae* (order *Bunyavirales*, family *Tospoviridae*), a devastating plant-pathogenic virus commonly referred to as tomato spotted wilt virus (TSWV). The larval gut is the gateway for virus transmission by *F. occidentalis* adults to plants. In a previous report, gut expression at the transcriptome-level was subtle but significant in response to TSWV in L1s. Since it has been well documented that the relationship between the expression of mRNA and associated protein products in eukaryotic cells is often discordant, we performed identical, replicated experiments to identify and quantify virus-responsive larval gut proteins to expand our understanding of insect host response to TSWV. While we documented statistically-significant, positive correlations between abundance of proteins (4,189 identified) and their cognate mRNAs expressed in first and second instar guts, there was virtually no alignment of individual genes identified to be differentially modulated by virus infection at the transcriptome and proteome levels. Predicted protein-protein interaction networks associated with clusters of co-expressed proteins revealed wide variation in correlation strength between protein and cognate transcript abundance, which appeared to be associated with the type of cellular processes, cellular compartments, and network connectivity represented by the proteins. In total, our findings indicate distinct and dynamic regulatory mechanisms of

transcript and protein abundance (expression, modifications, and/or turnover) in virus-infected gut tissues. This study provides molecular candidates for future functional analysis of thrips vector competence and underscores the necessity of examining complex virus-vector interactions at a systems level.

Keywords: western flower thrips; tomato spotted wilt virus; insect gut tissue; virus-vector interactions; weighted gene co-expression network analysis

1. Introduction

Quantitative measurements of molecular species, such as RNA and protein, are essential for dissecting molecular mechanisms in disease biology. mRNA abundance in cells has been commonly used as a proxy for protein expression (Vogel and Marcotte, 2012), however, the accumulating body of evidence generated from animal systems with numerous genomics data sets clearly shows that the correlation of mRNA and protein levels varies significantly across cell types (Du et al., 2019) and transcript abundance insufficiently predicts protein abundance (Liu et al., 2016; Payne, 2015). This context-dependent and discordant association between mRNA and protein levels has been ascribed to a variety of complex regulatory mechanisms, including post-transcriptional and post-translational silencing, mRNA decay and protein degradation (Gygi et al., 1999; Vogel and Marcotte, 2012). As such, it is imperative to investigate both transcriptional and translational events and/or outcomes in order to gain more precise views of host cellular, tissue system and physiological responses associated with pathogen invasion.

Orthotospovirus tomatomaculae, in the genus *Orthotospovirus* (family *Tospoviridae*, order *Elliovirales*) and commonly known as tomato spotted wilt virus (TSWV), causes severe damage on many economically important food crops. It is transmitted by the western flower thrips, *Frankliniella occidentalis* (Pergande), in a circulative-propagative manner. The first (L1) and early second instar (L2) larval thrips are critical to the virus transmission cycle because adults - the most significant plant inoculators of TSWV during probing and feeding in the landscape - are only vector competent if they acquire TSWV as young larvae (Moritz et al., 2004; Van De Wetering et al., 1996). Upon entry of the L1 midgut, the virus replicates and spreads throughout surrounding visceral gut muscles and disseminates to the salivary glands during the

49 late L2 stage. Virus is retained, albeit at lower abundance during the pupal stages (Schneweis et al., 2017),
50 and when adults eclose, virus increases in the adult principal salivary glands (Montero-Astúa et al., 2016b).
51 The virus is inoculated into the plant through thrips feeding (Montero-Astúa et al., 2016b; Ullman, 1992;
52 Ullman et al., 1995, 1993). Virus infection and replication of this circulative virus in thrips offers
53 opportunities for unraveling complex tissue response to infection. Considering the critical role of larval
54 guts for successful establishment of infection, unveiling molecular responses to virus invasion of this tissue
55 system is a significant step toward devising novel crop disease control strategies that disrupt the gut-virus
56 interaction.

57 Numerous studies have utilized next-generation sequencing to investigate the molecular aspects of
58 interactions between insect vectors and their associated plant viruses (Dietzgen et al., 2016; Ghosh and
59 Ghanim, 2021; Heck, 2018; Rotenberg et al., 2015). However, only a handful of studies have examined the
60 effect of plant virus infection on the gut of vector species (Brault et al., 2010; Geng et al., 2018; Han and
61 Rotenberg, 2021; W. Zhao et al., 2016). Previously, we reported the first thrips gut transcriptome of *F.*
62 *occidentalis* larvae in response to TSWV infection (Han and Rotenberg, 2021), and provided several
63 candidate biomarkers of infection at a stage when TSWV is known to enter and invade the epithelium of
64 the anterior midgut of L1 (*i.e.*, limited to a few cells) (Badillo-Vargas et al., 2019; Montero-Astúa et al.,
65 2016b), and when virus titer is at its lowest during the transmission cycle (Badillo-Vargas et al., 2012; Han
66 and Rotenberg, 2021; Rotenberg and Whitfield, 2018). It was the early L1 stage - three hours after a 24-
67 hour exposure period on TSWV-infected plant tissue – that exhibited a relatively larger transcriptome-wide
68 response to infection compared to the L2 stage (48 hours post exposure), when virus titers in the gut had
69 increased 3-fold (Han and Rotenberg, 2021), and virus has disseminated and invaded other regions of the
70 midgut (Montero-Astúa et al., 2016b).

71 This study attempts to gain a deeper understanding of the larval gut-TSWV interaction by i)
72 quantifying modulation of the gut proteome by the virus; ii) identifying protein co-expression networks and
73 functional enrichments represented by network members; and iii) examining the association between the
74 gut proteome (this study) and transcriptome of TSWV-exposed and non-exposed larval thrips, as well as

75 within network protein-transcript abundance correlations, by capitalizing on previously published gut
76 transcriptome data. Collectively, our analyses revealed distinct responses of thrips gut tissues to virus
77 infection at transcriptional and translational levels, stressing the importance of investigating virus-vector
78 interactions using complementary approaches.

79 **3. Results and Discussion**

80 **3.1. TSWV proteins detected in larval guts.** Comparisons were made between the first instar larvae, three
81 hours after a 24-hour exposure time to TSWV-infected plant tissue (3-L1-V) and second instar larvae
82 ensuing from the 3-L1 cohort, 48 hours after removal from the infected plant tissue (48-L2-V). Structural
83 and nonstructural proteins encoded by the five open reading frames of the TSWV genome were identified
84 in the gut proteome. We documented a significantly greater normalized abundance of nucleocapsid protein
85 (N, $P = 0.005$), a virion structural protein, and two non-structural viral proteins (NSs, $P = 0.036$ and NSm,
86 $P = 0.003$), in 48-L2, compared to 3-L1 of virus-exposed insects (**Figure 1**). Virus accumulation in thrips
87 guts after removal of the source of inoculum coupled with an increased abundance of non-structural proteins
88 is indicative of virus replication (De Assis Filho et al., 2002; Ohnishi et al., 2001; Ullman et al., 1993).
89 Increases in viral RNA (TSWV-N) from L1 to L2 bodies (Badillo-Vargas et al., 2012; Schneweis et al.,
90 2017) or guts (Han and Rotenberg, 2021) of *F. occidentalis* during growth and development have been
91 reported previously, corroborating our findings at the protein level.

92 While all attempts were made to avoid cross-contamination of virus-exposed (V) and non-exposed
93 (NV) samples during tissue dissection and sample processing, there were peptides at low occurrence and
94 low abundance that identified TSWV proteins in the NV-larval gut samples (**Supplementary File 1: Figure**
95 **S1.A-B**). We examined the possible origin of these peptide sequences in the NV samples by i) performing
96 NCBI blastp queries of the non-redundant protein database (Feb 13, 2024) using a low e-value cutoff (0.1)
97 to rule out possible matches to other organismal proteins that may have been present in the gut samples, ii)
98 performing local blastp queries to protein sequences retrieved from the NCBI Viral RefSeq Project
99 (Bioproject PRJNA485481) for viromes identified in *F. occidentalis* (52 proteins) and *Thrips tabaci* (118

100 proteins) (Chiapello et al., 2021), including bunyaviruses, that may have been harbored by our thrips isolate,
101 and iii) querying the *F. occidentalis* proteome with the identified TSWV peptides to rule out occurrence of
102 identical thrips peptide sequences. Based on these *post priori* analyses, there was no apparent evidence of
103 identical or similar peptide matches to other organisms or *F. occidentalis*. Of the 105 TSWV peptides
104 identified in this study overall, 23 aligned to protein sequences of other bunyaviruses reported for thrips
105 viromes. However, only ~50% of TSWV peptide query lengths (7 – 32 amino acids), on average, aligned
106 to any bunyavirus sequence match (N, NSs, NSm, or RdRP sequences). Moreover, 79% of the bunyavirus-
107 aligned peptides were mismatched in annotation (e.g., N peptide with RdRP peptide). Since the NV sample
108 peptides were identical in sequence and annotation to TSWV proteins, and only remotely aligned to other
109 thrips-harbored bunyaviruses, we attribute their occurrence to some source or means of TSWV protein
110 contamination during sample processing.
111
112 **3.2. Influence of larval developmental stage and virus on normalized protein abundance in the gut**
113 **proteome.** Our proteomic study detected a total of 47,169 unique peptides across all gut samples, which
114 identified 4,189 different *F. occidentalis* proteins. Principal component analysis (PCA) on a correlation
115 matrix of normalized thrips protein abundance values by larval stage-treatment groups (NV and V) revealed
116 that larval stages (3-L1 vs 48-L2), regardless of treatment, clustered separately along PC1, which explained
117 the majority of the variation in the data set (35.37%), and that 3-L1 clustered by virus infection status (NV
118 vs V) along PC2 (15.95% of the variation) (**Supplementary Figure S1A**). The finding that virus exposure
119 and/or infection had a subtle effect on the gut proteome compared to the physiological status of the thrips
120 vector is consistent with a report that *F. occidentalis* sex (male vs female adults) had a larger influence on
121 the salivary gland proteome than TSWV infection of these adult glands (Rajarapu et al., 2022). Supporting
122 the PCA observations, hierarchical clustering analysis revealed that samples grouped by both larval stage
123 and virus infection status, further underscoring the dual influence of developmental stage and viral factors
124 on the thrips gut proteome (**Supplementary Figure S1B**).
125

126 **3.3. Differential abundance of larval gut proteins in response to virus**. The larval gut response to TSWV
127 significantly modulated the abundance of 233 and 121 proteins expressed in 3-L1 and 48-L2 guts,
128 respectively (**Figure 2A**; $P < 0.05$ and at least 2-fold change compared to NV guts), referred herein as virus-
129 modulated, differentially abundant proteins (vDAPs, **Supplementary File 1: Table S2**). Comparatively,
130 the number of vDAPs in the *F. occidentalis* larval guts indicated a more robust gut response to TSWV
131 exposure and infection in 3-L1 compared to 48-L2 (**Figure 2A**). This finding is consistent with our previous
132 gut transcriptome study (Han and Rotenberg, 2021), where twice as many transcript sequences were
133 differentially-abundant in guts of 3-L1 (105) compared to 48-L2 (49). Notably, virus exposure led to a
134 greater apparent perturbation of gut proteins (relative numbers) compared to transcripts. The temporal
135 proximity of exposure to and acquisition from the TSWV-infected plant host for the 3-L1 cohorts (3 hours
136 post-removal of inoculum source) may, in part, explain the relatively larger response of L1s to the virus
137 treatment. Within the time-frame of the present study, gut infection of young L1s is localized to epithelial
138 cells of the anterior midgut, and within the L2 stage, TSWV has spread to other regions of the midgut and
139 surrounding visceral muscles. This well documented phenomenon of tissue tropism (reviewed in Montero-
140 Astúa, Stafford, et al., 2016), and the relative abundance of TSWV proteins in L1 compared to L2 guts
141 (**Figure 1**) did not appear to explain the more robust effect of TSWV on L1s. We hypothesize that ingestion
142 of infected plant tissue contributes to the larger gut response in L1s compared to L2s, which were sampled
143 48 hours after removal of the source of inoculum (~24 hours post molting from L1 to L2). Examination of
144 indirect (infected plant) vs. direct effects of TSWV on gut physiology is warranted to fully understand the
145 nature of the virus-vector interaction.

146 A great number of vDAPs in 3-L1 guts (62%) were predominantly down-regulated (**Figure 2B**),
147 as was reported for a whole-body proteome study of *F. occidentalis* L1s infected with TSWV (Badillo-
148 Vargas et al., 2012). In contrast, the 48-L2 guts showed a relatively equal distribution of up- and down-
149 regulated vDAPs. Of the 30 vDAPs determined to be shared between the two larval stages in the present
150 study (**Figure 2B**, **Supplementary File 1:Table S3**), mothers against decapentaplegic homolog 4 (Smad4)
151 and alpha-tubulin showed the most reduced abundances (**Figure 2C**) in both 3-L1 and 48-L2 guts. Smad4

152 is a signal transducer that mediates TGF-β signaling, regulating key genes involved in diverse physiological
153 processes, including cell proliferation, homeostasis, differentiation, apoptosis, and immune response
154 (Massagué, 2012). The significant down-regulation of Smad4 [log2 fold change (FC) ~ -7] could disrupt
155 TGF-β signaling pathways, which may have implications for gut immunity or stress responses during
156 infection. TGF-β signaling is known to exert both suppressive and stimulatory effects on pathogen
157 infections (reviewed in Deng et al., 2024). For example, studies have demonstrated that TGF-β1 enhances
158 rubella virus and Zika virus infections in human cells through the Smad pathway (Pham et al., 2021; Trinh
159 et al., 2022). However, the role of Smad4 in promoting or inhibiting TSWV infection in gut epithelial cells
160 requires further investigation. Alpha-tubulin is a structural, cytoskeletal protein that forms microtubules
161 (MT), adaptable tube-like structures that can rapidly reorganize, extend and depolymerize under different
162 physiological states and external stimuli (Desai and Mitchison, 1997; Gasic et al., 2019). Depolymerization
163 of microtubules (reviewed in Ohi et al., 2021) can lead to tubulin mRNA instability (Gasic et al., 2019) and
164 subsequent reduced tubulin synthesis (Ben-Ze'ev et al., 1979), referred to as tubulin autoregulation.
165 Autoregulation may have contributed to the reduced abundance of tubulins in guts of TSWV-infected L1s.
166 Tubulin cytoskeletal networks in animal cells have been implicated in virus attachment to cell surfaces,
167 intracellular trafficking, and virus replication (Naghavi and Walsh, 2017). More proximal to the present
168 study, rice stripe virus (RSV), a circulative-propagated, plant-pathogenic RNA virus, was shown to
169 upregulate and utilize alpha-tubulin for accumulation and dissemination along the route from gut cells to
170 salivary glands of the small brown planthopper (Li et al., 2020). Negative regulation of tubulins in TSWV-
171 infected L1 whole body proteomes (Badillo-Vargas et al., 2012) and the transcriptome of pro-pupae (P1)
172 of *F. occidentalis* (Schneweis et al., 2017) is consistent with the present findings of larval gut tubulins.
173 Other stage-shared proteins in the present study infer roles in DNA replication, transcription, intracellular
174 transport, protein and mRNA turnovers, stress response, lipid, nucleotide, and amino acid metabolisms,
175 detoxification, and cell cycle and structure (**Figure 2C, Supplementary File 1: Table S3**).

176 While many stage-shared vDAPs (63%) showed concordant direction of changes, others displayed
177 opposite regulations between 3-L1 and 48-L2, which suggests a shift in the gut's physiological or immune

178 response as infection progresses (**Figure 2C**). For the most part, these shared proteins and their associated
179 normalized abundances under the infection state indicate a negative regulation of gene expression and/or
180 enhanced protein turnover in 3-L1 guts. However, this trend was inverted in 48-L2 guts, where most
181 proteins were up-regulated. If and how TSWV modulates these cellular processes in thrips vector cells
182 remains to be determined, and the current lack of a robust, immortalized thrips cell line for research beckons
183 us to innovate ways to address these basic questions.
184
185 **3.4. Gene ontologies (GO) and functional enrichment of larval gut proteins in response to TSWV**. Of
186 the 324 non-redundant vDAPs identified across the two larval stages, 79% were assigned GO terms
187 (**Supplementary Figure S2, Supplementary File 1: Table S2**). The most predominant GO annotations in
188 the biological process (BP) were 'transport' and 'regulation of cellular process' for 3-L1 and 48-L2 guts,
189 respectively. In the molecular function, 'hydrolase activity' was the most common annotation for both
190 stages. The most frequent cellular compartments assigned to the vDAPs were 'membrane' for 3-L1 guts
191 and 'protein-containing complex' for 48-L2 guts. Using STRING, it was determined that 82% and 73% of
192 the thrips vDAP sequences for the 3-L1 and 48-L2 guts, respectively, identified orthologs (279 in total) in
193 the annotated *D. melanogaster* proteome, and GO enrichment analysis of these orthologs revealed more
194 granular, functional annotations encompassed by the mapped vDAPs (**Figure 3, Supplementary File 1:**
195 **Table S4**). Not surprisingly, GO terms for the collection of vDAPs mirrored those of the larval stage overlap
196 (DNA replication, nucleic acid metabolism, and cell structure) (**Figure 2C**).
197 Other enriched GO terms were revealed, namely 'cellular component organization or biosynthesis'
198 and 'primary metabolic process' (**Figure 3**). We found that a vast majority of cellular component-associated
199 vDAPs were down-regulated in larval gut tissues after virus infection. The 3-L1 guts exhibited a more
200 pronounced cellular response than 48-L2 guts (65 vs 23 vDAPs). The most perturbed gut protein in this GO
201 term was cytoplasmic FMR1-interacting protein-like isoform X1 (Cyfip, FC = -563.98), involved in actin
202 cytoskeleton reorganization, mRNA translation, and endocytic trafficking and signaling (Abekhoukh et al.,
203 2017; Napoli et al., 2008; Zhao et al., 2013). The substantial down-regulation of Cyfip in thrips guts may

204 impair the cytoskeletal dynamics of gut epithelial cells, which are essential for maintaining gut structure
205 and function. Among the up-regulated vDAPs, the F-box only protein 11 (FBXO11) showed a 40.41-fold
206 increase in abundance in 3-L1 guts following virus infection. FBXO11 is a subunit of a SCF E3-ubiquitin
207 ligase complex involved in degradation of diverse cellular proteins and has been implicated in silencing by
208 si- and miRNAs at the step of RISC-loading in *Drosophila melanogaster* (Lee et al., 2009). More recently,
209 it was reported that silencing of USB7 (a E3-ubiquitin ligase) in *F. occidentalis* adults resulted in reduced
210 virus transmission to the host, but had no effect on acquisition (i.e., larval gut) (Shi et al., 2023).

211 In the enriched GO term of 'primary metabolic process', there were 83 and 40 vDAPs classified in
212 the 3-L1 and 48-L2 guts, among which 66% and 48% were down-regulated, respectively (**Figure 3,**
213 **Supplementary File 1: Table S4**). This category represented proteins with roles in protein ubiquitination
214 or deubiquitination (proteolysis), DNA replication and repair, transcription regulation, regulation of mRNA
215 splicing, ribosome biogenesis and translation, signal transduction, and lipid metabolism. vDAPs at the
216 extremes in magnitude in change in response to TSWV for this GO term (**Figure 3**) were ValRS (FC = -
217 587.10), a valine-tRNA ligase known for its role in protein synthesis by incorporating valine into proteins,
218 and verm (FC = 255.15), a chitin deacetylase involved in chitin remodeling and insect molting. Chitin is a
219 key component of the cuticle and peritrophic membrane (PM) lining the midgut epithelium of many insects
220 (Zhu et al., 2016). Cuticular proteins have shown to play an important role in virus transmission in diverse
221 vector-borne plant virus systems. Unlike insects with PMs, hemipteran and thysanopteran midguts are lined
222 with perimicrovillar membranes (PMMs) (Silva et al., 2004). Previously, Badillo-Vargas and Chen
223 demonstrated that three cuticular proteins, containing chitin-binding domains, interacted directly with
224 TSWV glycoprotein (G_N) and were abundantly expressed in thrips guts and salivary glands. They
225 hypothesized that chitin or chitin-like structures might be integrated into the PMM and salivary gland
226 linings of thrips (Badillo-Vargas et al., 2019). Based on this hypothesis, we propose that the significant up-
227 regulation of verm in 48-L2 guts may accelerate the conversion of chitin to a more soluble and less rigid
228 chitosan polymer. This modification could potentially increase the permeability of the PMM lining, altering

229 the gut environment in ways that may support TSWV replication or movement. In total, these vDAP
230 identified orthologs with known, conserved functions with vital roles in cell biology and virology.
231
232 **3.5. Larval gut co-expression protein networks.** Using the collection of all *F. occidentalis* larval gut
233 proteins identified in this study (4,189), WGCNA revealed a total of nine distinct clusters (i.e., modules) of
234 co-expressed proteins grouped into four branches of the eigengene dendrogram, referred to as meta-
235 modules (Langfelder and Horvath, 2008) (**Figure 4A**). vDAPs were distributed across eight modules, with
236 the 'turquoise' module containing the most (112), 92% of which were down-regulated in response to TSWV
237 (**Supplementary File 1: Table S2**). Modules that were positively correlated (**Figure 4B**, $P < 0.05$) with
238 the TSWV condition were the 'darkgreen (14% of vDAPs) and 'darkgrey' (11% of vDAPs) modules, and
239 all of the vDAPs in these modules (87) were more abundant (up-regulated) in response to virus (3-L1 and
240 48-L2), with the exception of the sole two (down-regulated) associated with the 48-L2 stage
241 (**Supplementary File 1: Table S2**). The 'darkgreen' and 'darkgrey' modules of proteins resided in two
242 different meta-modules, suggesting different biological roles (Langfelder and Horvath, 2008) with regards
243 to perturbation by the virus condition.
244 Network membership analysis of the 'darkgreen' (192 proteins in total) and 'darkgrey' (420
245 proteins in total) modules identified 15 and 33 highly interconnected hub proteins, respectively (**Figure 5**),
246 each with a module membership value (kME) no less than 0.86 and the greatest number of intramodular
247 connections (kIN > 41) (**Supplementary File 1: Table S5**). All, except one, of the 'darkgreen' hub proteins
248 were vDAPs (**Figure 5B)**, while only one of the 'darkgrey' hubs were responsive to TSWV under our
249 experimental conditions (**Figure 5D**). Given that these hub proteins share the most connections with other
250 co-expressed proteins (including other hubs), they likely play a critical role in regulating or coordinating
251 activities of 'neighborhood' proteins in response to viral activities in larval gut cells.
252 Systems-level analyses of disease-associated omics datasets have led to the identification of key
253 molecular pathways and potential new targets and biomarkers of diseases (Altaf-Ul-Amin et al., 2014).
254 Functional analysis of the hub proteins and their connecting proteins with regards to thrips biology and

255 thrips vector competence warrants further study. For example, in the present study, FOCC009188
256 (abbreviation: F9188), an uncharacterized protein with unknown function, was identified as a hub protein
257 in the 'darkgreen' module. Notably, it was also shown as the most connected central hub gene in a co-
258 expression network that was enriched with TSWV-responsive transcripts in *F. occidentalis* larval guts (Han
259 and Rotenberg, 2021). Moreover, its protein abundance was significantly up-regulated in both 3-L1 and 48-
260 L2 guts after virus infection, and its corresponding mRNA was previously shown to be ~3-fold higher in
261 TSWV-infected 3-L1 guts compared to uninfected controls.
262
263 **3.6. Comparative analysis of the proteomes and transcriptomes of the larval gut of TSWV-exposed**
264 **and non-exposed thrips**. Identifiers (FOCC gene IDs) of all non-redundant larval gut proteins identified
265 (4,189) were used to recover their associated transcripts and normalized abundance values from a
266 previously published RNA-Seq expression data set for *F. occidentalis* larval transcriptomes under V and
267 NV conditions (Han and Rotenberg, 2021) (**Supplementary File 1: Table S6**). To ensure the highest level
268 of experimental consistency between the RNA-seq and proteomics analyses, our proteome experiment was
269 meticulously designed and executed in strict accordance with the protocols defined in our RNA-Seq study.
270 The search recovered transcript expression data for 99.3% of the protein data set. Statistical analysis of the
271 paired transcript-protein expression data ($\log_2$ normalized abundance) revealed significant, positive
272 correlations (Pearson, r) for guts of the 3-L1 ($r = 0.625$, $P < 0.0001$) and 48-L2 ($r = 0.583$, $P < 0.0001$)
273 larval stages. Correlations of this strength and significance are remarkable for heterogeneous gut tissue
274 (diverse cell types) that represent different regions of the insect gut (foregut, midgut and hindgut).
275 Regression analyses on (x, y) pairs of TSWV-modulated proteins for each virus condition (NV/V) revealed
276 a more significant, yet weak association between protein and transcript abundance in V-3-L1 guts ($R^2 =$
277 18.1, $P < 0.0001$, $n = 228$) compared to NV-3-L1 ($R^2 = 0.11$, $P = 0.265$, $n = 228$) guts (**Figure 6B vs 6A**).
278 Despite significant positive correlations in larval guts in general, use of transcript abundance to explain the
279 variation in protein abundance had limited value for TSWV-modulated proteins.

280 The two ‘omics expression datasets were cross-queried (by OGS IDs) to identify overlapping
281 sequences that were significantly ($P < 0.05$) perturbed by TSWV as compared to NV counterparts. In each
282 stage, only two sequences were shared between the data sets, with all agreeing in the direction of changes
283 in both protein and transcript levels (**Table 1**). Among them, FOCC000766 was further shared between 3-
284 L1 and 48-L2 guts and consistently down-regulated in both stages. This sequence was annotated as
285 phospholipase A1-like (PLA1), which functions in lipid metabolism, signal transduction, and membrane
286 remodeling (Richmond and Smith, 2011). Down-regulation of PLA1 activity may impact lipid remodeling
287 and cellular membrane properties, facilitating virus infection and dissemination in gut epithelium. The other
288 two sequences were uncharacterized proteins with unknown functions (**Table 1**); however, FOCC009188
289 stands out as a particularly strong candidate for further investigation due to its consistent responses to virus
290 infection and intramodular hub centrality within co-expressed protein and transcript modules (Han and
291 Rotenberg, 2021) (**Figure 5B**).

292 Among the 324 non-redundant vDAPs, 99% displayed unaltered mRNA abundances after virus
293 exposure, implying undisturbed transcription while post-transcriptional processes influenced translation
294 efficiency (Sunnerhagen, 2007; B. S. Zhao et al., 2016). This gave rise to variable translation, with some
295 proteins being enhanced and others diminished. Similarly, among the 147 non-redundant, differentially-
296 expressed transcripts from our previous gut transcriptome study (Han and Rotenberg, 2021), 98%
297 maintained stable protein levels despite potential fluctuations in mRNA levels. This protein stability may
298 arise from adjustments in translation rates, changes in mRNA stability, and post-translational modifications
299 like phosphorylation, ubiquitination, or acetylation, ensuring protein constancy even in the face of shifting
300 mRNA abundances (Deribe et al., 2010; Mata et al., 2005; McCarthy, 1998; Pradet-Balade et al., 2001).
301 Collectively our data indicates distinct transcriptional and translational responses of the larval gut to TSWV
302 infection, given that consistent experimental conditions, parameters, and timing were followed intentionally
303 for the two ‘omics studies. These distinct responses likely reflect temporally-dynamic and direct physical
304 and biochemical interactions between the bunyavirus and host cell machinery, molecular building blocks
305 (nucleotides and amino acids), and myriad unknown host factors available in the cytoplasm to complete its

306 'life-cycle' [transcription, translation, replication, virion assembly] (reviewed in Elliott & Schmaljohn,
307 2013). TSWV-induced, post-translational modifications of host proteins (Gong et al., 2023) may also
308 contribute to the discordance between transcriptomic and proteomic response. Mass spectrometry-based,
309 discovery proteomics methodologies, such as the one used in the present study, are not designed to handle
310 identification of PTMs (Kim et al., 2016), especially with the use of a reference proteome database
311 composed of single protein models per gene model. Therefore, use of existing RNA-Seq datasets for *F.*
312 *occidentalis* in public repositories to identify transcript variants and isoforms for gene models and
313 incorporation of PTM detection techniques for new proteome datasets may provide a more complete view
314 of host response to virus or other persistent perturbations.
315
316 **3.7. Intramodular analysis of correlations between protein and transcript abundance, and functional**
317 **enrichment.** In an attempt to approach the basis of correlations between transcriptome and proteome
318 expression patterns in larval guts, rank correlation coefficients (Spearman's rank coefficient, ρ) were
319 calculated for protein-transcript pairs for the nine sets of module members for each larval stage-treatment
320 combination. The analyses revealed significant, positive associations (ρ) for all the nine modules. However,
321 the strength of the association varied considerably among these modules (**Figure 7**).
322 Functional enrichment analyses of protein-protein interactions (PPI) in five module networks were
323 performed, one of which represented the highest strength in protein-transcript associations in the data set
324 [grey60 (mean ρ = 0.821)], the two [darkgrey (mean ρ = 0.682) and darkgreen (mean ρ = 0.413)] that were
325 significantly (positive) associated with TSWV (**Figure 4B**), and the two [darkred (mean ρ = 0.607) and
326 cyan (mean ρ = 0.575)] that showed distinct protein-transcript correlation strengths between 3-L1 and 48-
327 L2 guts (**Figure 7**). A summary of the functional enrichments and associated metrics for these five networks
328 is presented in **Supplementary File: Table S7.** The grey60 network (232 nodes) was enriched ($P < 1x10^{-}$
329 ^{16}) in ribosomal proteins and other highly conserved translational machinery and translation factors (e.g.
330 eukaryotic elongation factors). The darkgrey network (346 nodes) was enriched ($P < 1x10^{-16}$) in proteins
331 associated with mitochondrial structure and processes, including pyruvate metabolism and ATP synthesis

332 (pyruvate dehydrogenase complex), electron transport and energy production (iron-sulfur cluster binding),
333 and fatty acid beta-oxidation and protein phosphorylation. The darkgreen network (145 nodes) had
334 relatively fewer member connections (no. of edges in relation to no. of hubs) compared to the other modules
335 of comparable neighborhood size, and functional enrichment was statistically supported, albeit at a lower
336 significance ($P < 1.8^{-3}$). It was enriched for functions associated with the TRAPPIII protein complex, a key
337 regulator of intracellular membrane trafficking from the endoplasmic reticulum to the Golgi apparatus,
338 particularly in the secretory pathway and autophagy. The darkred network (305 nodes) was enriched ($P <$
339 $1x10^{-16}$) in proteins related to mitochondrial processes, fatty acid metabolism, proteasome activity, and
340 virus entry regulation. The cyan network (349 nodes) was enriched ($P < 1x10^{-16}$) in proteins involved in
341 processes, such as mitochondrial fission, fatty acid elongation, proteasome degradation, and storage
342 proteins. The darkred network features a more prominent role for clathrin and viral entry, suggesting a
343 potential involvement in trafficking and virus-host interactions, whereas the cyan network emphasizes
344 larval serum protein complexes and ER-associated processes, indicating a possible role in protein storage
345 and degradation. Both networks share a common theme: protein degradation, specifically through the
346 proteasome. This suggests that protein turnover is a critical process in both 3-L1 and 48-L2 guts. However,
347 the specific proteins targeted for degradation may differ between the two stages as evident by the reduced
348 correlations between mRNA and protein levels in 48-L2 guts (darkred mean $\rho = 0.537$, cyan mean $\rho =$
349 0.497) compared to 3-L1 guts (darkred mean $\rho = 0.678$, cyan mean $\rho = 0.654$) (**Figure 7**).

350 WGCNA-derived modules represent different sets of interconnected genes, and by virtue of these
351 connections, indicate coordinated interactions that culminate into distinguishable cellular processes. Based
352 on the intramodular correlations between protein and transcript abundance and functional enrichments
353 determined by our analyses, we posit that the strength of the transcript-protein association may be
354 explained, in part, by the type of cellular processes and cellular compartmentalization represented by the
355 module (Du et al., 2019; Tasaki et al., 2022), and possibly connectivity (number of connections) of a protein
356 with other proteins within the PPI network, like conserved translational and post-translational machinery
357 (e.g., ribosomal protein complexes, proteasome) (Tasaki et al., 2022). Indeed, the enrichment of the grey60

358 and darkgrey networks with translation elongation factor complexes and mitochondrial compartmentalized
359 proteins, respectively, is consistent with this hypothesis, as is the darkgreen network with fewer PPI edges
360 and enrichment in proteins that play roles in intracellular membrane trafficking and autophagy. One study
361 addressed the discordance of transcript to protein abundance by training models on cancer tumor 'omics
362 datasets and validating the predictive power of non-cognate transcript abundance on proteins in large and
363 small multiprotein complexes associated with diverse biological processes (Srivastava et al., 2022).
364 Determination of transcript variants and post-translational modifications in tissues of *F. occidentalis* and/or
365 other thrips vectors of orthotospoviruses may provide a pathway towards identification of reliable
366 biomarkers of vector competence, significantly advancing our understanding of virus transmission by thrips
367 vectors.

368 **3. Experimental Procedures**

369 **3.1 Biological source for larval gut protein samples.** The source of *F. occidentalis* (lab colony on green
370 bean pods), isolate of TSWV (*Emilia sonchifolia* lab culture), and the TSWV acquisition protocol – i.e.,
371 age-synchronized L1 cohorts subjected to a 24-hour acquisition access period (AAP) on infected (V) or
372 non-infected (NV) plant tissue, then moved to green beans for gut clearing and development - were prepared
373 and used precisely as described for our larval gut transcriptome study (Han and Rotenberg, 2021). The gut
374 proteome experiment consisted of the two treatments (V and NV) and two sampling time-points post AAP
375 [3-hrs (L1 stage) and 48-hrs (L2 stage), and the experiment was conducted three independent times (i.e.,
376 biological replicates) (**Supplementary Figure S3**). Infection rates of larval cohorts (V and NV) were
377 determined by arbitrarily subsampling 10 individuals (L1) and subjecting each larval body to RNA
378 extraction and cDNA synthesis followed by real-time PCR detection of TSWV nucleocapsid (N) RNA and
379 *F. occidentalis* actin RNA (internal reference) as described previously (Han and Rotenberg, 2021). Based
380 on this strategy, it was confirmed that each V cohort (all three bio-replicates) exhibited a 100% infection
381 rate, and TSWV N RNA was not detected in the NV cohorts.

382 **3.2. Thrips gut dissection.** To ensure the highest level of experimental consistency for comparing proteome
383 expression data to the published RNA-seq dataset (Han & Rotenberg, 2021), we executed experiments and
384 thrips dissections in strict accordance with the protocols that formed the basis for the RNA-seq study,
385 including taking into account possible effects of diurnal cycles on gene expression (e.g., all gut dissections
386 performed at same period during the day). Larval dissections were performed to carefully remove gut tissue,
387 which included the foregut, midgut, and partial hindgut as described previously (Han and Rotenberg, 2021),
388 with adaptations for downstream protein analyses. A detailed experimental design is illustrated in
389 **Supplementary Figure S3** in the current study. Each thrips larva was placed on a sterile microscope slide,
390 immersed in ice-cold phosphate-buffered saline (PBS) buffer (~80 µl), then decapitated using a sterile,
391 polymer-coated scalpel blade (#15, Southmedic Inc., Barrie, Ontario, Canada). Undesired tissues, including
392 principal and tubular salivary glands, fat body, and other residual body parts were carefully removed from
393 the gut tissue using an ultrafine single deer hair tool (Ted Pella, Redding, CA). After dissection, an
394 additional ice-cold PBS buffer (~100 µl) was added to the slide to further wash away the unwanted residual
395 tissue and body contents from the gut tissue. Each gut was immediately pulled through the surface of the
396 buffer with the single deer hair tool and transferred into 200 µl of fresh ice-cold PBS buffer in a sterile 1.5-
397 ml microfuge tube. This process was repeated to pool a total of 100 guts in the same tube, which was placed
398 on ice throughout the entire process. Each replicate of the experiment was performed under the same
399 laboratory conditions, during the same time period of the day, and by alternating between 20 NV-larvae
400 and 20 V-larvae until obtaining 100 guts for both samples (using separate tools for each treatment). Sample
401 tubes containing gut tissues were centrifuged at 8,000 g for 5 minutes and excess PBS buffer was carefully
402 removed to achieve 20 µl in each tube. Gut samples were immediately flash-frozen in liquid nitrogen and
403 stored at -80°C until use. A total of 12 gut samples were prepared (two treatments, two sampling time
404 points, three bio-replicates). To ensure that 100 guts would provide sufficient protein concentrations for
405 downstream processing, we performed the bicinchoninic acid assay (BCA) (Thermo Fisher Scientific,
406 Waltham, MA) to estimate total protein concentration on an entirely separate pool of 100 L1 guts.

407 **3.3. Tissue-processing and ultra-performance liquid chromatography-tandem mass spectrometry**
408 **analysis.** The 12 frozen gut samples were submitted to the Duke Proteomics and Metabolomics Core
409 Facility for sample processing and ultra-performance liquid chromatography-tandem mass spectrometry
410 (UPLC-MS/MS) analysis and mass spectrometry data acquisition using state-of-the-art proteomic tools,
411 resources and expertise. Briefly, each sample was spiked with undigested bovine casein as an internal
412 quality control standard, which were then supplemented with 100 µl of 8M urea/50 mM ammonium
413 bicarbonate. Proteins were solubilized by probe sonication (30% power, 3X). Protein content was estimated
414 based on the protein concentration determined by BCA assay, and 4.5 ng of protein extract was used for
415 enzymatic digestion with 20 ng/µl sequencing grade trypsin (Promega, Madison, WI) for 1 hour at 47°C,
416 and eluted using 50 mM TEAB, followed by 0.2% FA, and lastly using 50% ACN/0.2% FA. All samples
417 were then lyophilized to dryness and resuspended in 12 µl of 1% trifluoroacetic acid/2% acetonitrile with
418 12.5 fmol/µl of yeast alcohol dehydrogenase (ADH). A study pool quality control (SPQC) was created by
419 combining equal volumes of each sample.

420 Quantitative LC/MS/MS was performed with 4 µl of each sample using a nanoAcquity UPLC
421 system (Waters Corp) coupled to a Thermo Orbitrap Fusion Lumos high resolution accurate mass tandem
422 mass spectrometer (Thermo) equipped with a FAIMSPro device via a nanoelectrospray ionization source.
423 Samples were randomized across all four unique biological groups with sample pool QC standards run
424 periodically throughout the study window. This acquisition strategy is, in part, designed to access a "real
425 signal" across a large sample cohort, and provides support that the signals are not an artifact of the analytical
426 system or experimental design. Briefly, the sample was first trapped on a Symmetry C18 20 mm×180 µm
427 trapping column (5 µl/min at 99.9/0.1 v/v water/acetonitrile), after which the analytical separation was
428 performed using a 1.8 µm Acquity HSS T3 C18 75 µm×250 mm column (Waters Corp.) with a 90-min
429 linear gradient of 5 to 30% acetonitrile with 0.1% formic acid at a flow rate of 400 nl/min with a column
430 temperature of 55°C. Data collection on the Fusion Lumos mass spectrometer was performed for three
431 different compensation voltages (CV) (-40v, -60v, -80v). Within each CV, a data-dependent acquisition
432 (DDA) mode of acquisition with a r=120,000 (@ m/z 200) full MS scan from m/z 375-1500 with a target

433 AGC value of 4e5 ions was performed. MS/MS scans were acquired in the linear ion trap in "rapid" mode
434 with a target AGC value of 1e4 and max fill time of 35 milliseconds. The total cycle time for each CV was
435 0.66 seconds, with total cycle times of 2 seconds between full MS scans. A 20-second dynamic exclusion
436 was employed to increase depth of coverage. The total analysis cycle time for each sample injection was
437 approximately 2 hours.
438
439 **3.4. Mass spectrometry data acquisition and analysis.** Following 16 total UPLC-MS/MS analyses
440 (including four replicative SPQC samples), data were imported into Proteome Discoverer 2.4 (Thermo
441 Scientific Inc.) and individual UPLC-MS/MS data files were aligned based on the accurate mass and
442 retention time of detected precursor ions ("features") using Minora Feature Detector algorithm in Proteome
443 Discoverer. Relative peptide abundance was measured based on peak intensities of selected ion
444 chromatograms of the aligned features across all runs. The MS/MS data was searched against the combined
445 protein sequence database consisting of the *Frankliniella occidentalis* protein sequence database
446 (Rotenberg et al., 2019), tomato spotted wilt virus protein sequences [AAF80981.1 (G_N/G_C glycoprotein
447 precursor); AAL55403.1 (RNA-dependent RNA polymerase); in house clones for NSs, NSm, and N]; a
448 common contaminant/spiked protein database (bovine albumin, bovine casein, yeast ADH, etc.), and an
449 equal number of reversed-sequence "decoys" for false discovery rate (FDR) determination. Mascot Distiller
450 and Mascot Server (v 2.5, Matrix Sciences) were utilized to produce fragment ion spectra and to perform
451 database searches. Database search parameters included fixed modification on Cys (carbamidomethyl) and
452 variable modification on Met (oxidation). Search tolerances were 2 ppm precursor and 0.8 Da product ion
453 with full trypsin enzyme rules. Peptide Validator and Protein FDR Validator nodes in Proteome Discoverer
454 were used to annotate the data at a maximum 1% protein FDR based on q-value calculations. A peptide
455 matched to multiple different proteins was exclusively assigned to the protein that had more identified
456 peptides. Protein homology was addressed by grouping proteins that had the same set of peptides to account
457 for their identification. A master protein within a group was assigned based on percent coverage.

458 **Supplementary File: Table S8** provides raw peptide sequences, metrics (retention times, mass, ion scores)
459 and raw abundance values for the 16 total UPLC-MS/MS analyzed samples.

460 Prior to imputation, a peptide filter was deployed which required a peptide to have a measurable
461 quantitative value in >50% of the samples within a treatment group. After filtering, any missing values
462 were imputed using the following rules: 1) if only a single signal was missing within the group of three, an
463 average of the other two values was used, or 2) if two out of three signals were missing within the group of
464 three, a randomized intensity within the bottom 2% of the detectable signals was used. To summarize the
465 protein abundance, all peptides belonging to the same protein were summed into a single intensity. This
466 consolidation enhances the overall representation of protein abundance, contributing to a more
467 comprehensive analysis. The protein abundance data was then normalized using a robust mean
468 normalization, in which the highest and lowest 10% of the signals were excluded and the average of the
469 remaining signals were normalized to be the same across each individual channel.

470 In order to assess technical reproducibility, % coefficient of variation (%CV) was calculated for
471 ADH spiked into each sample prior to any type of data normalization. The variation was 19.0%, which is
472 well within expected for non-normalized spiked control data. Then, %CV was calculated for each protein
473 across four injections of the SPQC pool that were interspersed throughout the study. The mean %CV of the
474 SPQC pools was 9.0% which is well within expected analytical tolerances for this type of analysis. To
475 assess biological plus technical variability, %CVs were calculated for each protein, and mean %CV were
476 calculated to be 29.2%, 20.4%, 17.4% and 21.8% for NV-3-L1, V-3-L1, NV-48-L2, and V-48-L2,
477 respectively. Overall, these variations are well within the desired variations and indicate consistent protein
478 extraction, processing and data acquisition.

479 **3.5. Identification and annotation of virus-mediated, differentially abundant proteins (vDAPs).** A
480 two-tailed heteroscedastic *t*-test was employed to identify vDAPs in V guts compared to NV guts based on
481 normalized protein abundance and using the criteria of p-value < 0.05 and fold change ≥ 2. Amino acid
482 sequences of all vDAPs, i.e., non-redundant vDAPs identified across both larval developmental stages,

483 were subjected to Blastp to query the NCBI non-redundant protein database followed by mapping and
484 annotation with Gene Ontology (GO) terms (E < 1.0E-5) for three provisional functional GO categories
485 (biological process, molecular function, and cellular component) using OmicsBox v2.0 (Götz et al., 2008).
486 To further discriminate more specific putative roles, the vDAP amino acid sequence (one file containing
487 multiple fasta-formatted sequences) were subjected to STRING analysis (https://string-db.org/) (Szklarczyk
488 et al., 2023) to map vDAPs to the program-supplied, annotated *Drosophila melanogaster* proteome in order
489 to predict functional and physical protein networks and to identify significantly enriched functions
490 represented by the vDAPs.

491 **3.6. Weighted gene co-expression network analysis (WGCNA).** A matrix of $\log_2$-transformed,
492 normalized abundance values for all detected proteins (4,189) across the 12 gut samples were subjected to
493 WGCNA for identifying modules (clusters) of co-expressed proteins and their statistical associations with
494 an external sample trait, in this case, TSWV treatment (Langfelder and Horvath, 2008). The adjacencies
495 between proteins were calculated using a soft-thresholding power of 14 under the 'signed' network. The
496 adjacency matrix was transformed into a topological overlap matrix for calculating the corresponding
497 dissimilarity. Modules of co-expressed proteins were identified by applying the 'dynamic tree cut' method
498 with minimum module size set as 35. By virtue of including all gut proteins identified in the analysis,
499 modules have the potential to include both vDAPs (TSWV-responsive) and non-vDAPs (not responsive to
500 TSWV as compared to NV treatment). Similar modules were merged if their eigengenes shared at least
501 65% similarity. The module-trait relationships were analyzed by correlating module eigengenes and the
502 infection status (NV or V) of gut samples. Modules that were significantly associated with TSWV treatment
503 were further analyzed for identifying intramodular hub proteins. Proteins that ranked in the top 10% of both
504 module membership (kME, correlation of a protein to its module eigengene) and intramodular connectivity
505 (kIN, sum of connection weights between a protein with all its connected neighbors) among all module
506 proteins were considered as hub proteins. The intramodular interaction networks were visualized with
507 VisANT software v5.53 (Hu et al., 2004). In addition, as described above (section 3.5) for all DAPs,

508 STRING analyses were performed on module sequence sets that were determined to be significantly ($P <$
509 0.05) associated with the trait of TSWV treatment in order to identify enriched functional categories within
510 modules.

511 **3.7. Cross-datasets comparisons of transcriptomes and proteomes of *F. occidentalis* larval guts.**
512 Sequence identifiers (OGSv1.1, FOCC IDs) (Rotenberg et al., 2019a, 2019b) of all non-redundant proteins
513 identified in L1 and L2 guts were used to query a *F. occidentalis* larval (L1 and L2) gut transcriptome
514 sequence database assembled previously for a gut RNA-seq experiment (Han and Rotenberg, 2021) that
515 utilized the same insect and virus source, larval developmental stage-time of sample, experimental set-up,
516 conditions and personnel as implemented in the present study. A data matrix consisting of sequence
517 identifiers, sample factors [larval stage (3-L1, 48-L2), treatment (V/NV)], average (n=3) $\log_2$(normalized
518 transcript abundance) (x) and average (n=3) $\log_2$(normalized protein abundance) (y) was prepared.
519 Statistical correlation coefficients (Pearson, r) were calculated, and linear regression analyses were
520 performed on all x, y data (all proteins identified with a transcript match) and vDAPs only for each larval
521 stage – treatment combination to determine the strength and significance of the relationship between protein
522 and transcript abundance. Spearman rank correlation coefficients (ρ) were calculated for the sets of x, y
523 data associated for each WGCNA module of co-expressed proteins to examine the possible association
524 between enriched functions ascribed to a module and the strength of the association between protein-
525 transcript abundance. In addition, the list of TSWV-responsive transcripts identified in larval guts
526 previously (105 for 3-L1 and 49 for 48-L2) and gut DAPs identified here were examined for overlap. All
527 correlation and regression analyses were performed with JMP Pro v.15.

528 **Supplementary Materials:**

529 **Supplementary Figures.**

530 **Figure S1:** Principal component analysis and hierarchical clustering of *Frankliniella occidentalis* larval
531 gut samples (.pdf)

532

533 **Figure S2:** Distribution of TSWV-modulated, differentially-abundant proteins (vDAPs, up- and down-
534 regulated) into gene ontologies (GO) assigned for up- and down-regulated proteins identified in guts of 3-
535 L1 and 48-L2 stages (.pdf)
536
537 **Figure S3:** Experimental design for preparing *Frankliniella occidentalis* larval gut samples for the
538 proteomics study (.pdf)
539
540 **Supplementary File 1:** Workbook of supporting data figures and tables (Figure S1AB, Tables S2 – S8)
541 (.xlsx)
542
543 **Author Contributions:** Conceptualization, D.R and J.H..; methodology, D.R. and J.H.; formal analysis,
544 J.H. and D.R; investigation, J.H.; resources, D.R.; data curation, J.H.; writing-original draft preparation and
545 editing, J.H. and D.R.; visualization, J.H.; supervision, D.R.; project administration, D.R.; funding
546 acquisition, D.R.. All authors have read and agreed to the published version of the manuscript.

547 **Funding:** This research was supported by the NC Agricultural Research Service and by USDA National
548 Institute of Food and Agriculture grant no. 2018-67013-28495.

549 **Data Availability Statement:** The raw mass spectrometry datasets generated in this study have been
550 deposited in the MassIVE repository (https://massive.ucsd.edu/ProteoSAFe/static/massive.jsp) under
551 project ID: MSV000096811 (available upon publication).

552 **Acknowledgements.** We thank Dr. Erik Soderblum and his staff at the Duke University School of
553 Medicine, Proteomics and Metabolomics Core Facility, for providing consultation and state-of-the-art
554 services of sample processing, protein identification and normalization, and statistical analysis of
555 differential protein expression. We thank Swapna Priya Rajarapu for her assistance with virus acquisition

assays and discussions about best practices for thrips dissection for proteomics and data analysis. We also thank Drs. Marlonni Maurastoni and Anna Whitfield for internal review of the manuscript.

Conflicts of Interest: The authors declare no conflict of interest.

560 **Table 1.** Shared TSWV-responsive larval gut proteins and transcripts identified from the proteomics and
561 transcriptomics analyses

Stage[x]	ID	vDAPs[#]			DETs[&]			Gene description
		FC[$]	*P*-value	Regulation	FC	*P*-value	Regulation	
3-L1	FOCC009188	69.73	0.002	Up	3.18	0.008	Up	hypothetical protein FOCC_FOCC009188
	FOCC000766	-3.57	0.023	Down	-4.23	0.000	Down	phospholipase A1-like
48-L2	FOCC001083	-18.89	0.018	Down	-8.75	0.006	Down	hypothetical protein FOCC_FOCC001083
	FOCC000766	-3.27	0.047	Down	-5.86	0.021	Down	phospholipase A1-like

562

563 [X] developmental stage: 3-L1 = first instar larvae, 3 hours after a 24-hour exposure time on non-infected or
564 TSWV-infected plant tissue; 48-L2 = second instar larvae ensuing from the 3-L1 cohorts, 48 hours after
565 removal of non-infected or infected plant tissue; [#] vDAPs: virus-responsive, differentially abundant
566 proteins identified from this study; [&] DETs: differentially-expressed transcripts from a previous gut
567 transcriptome study (Han and Rotenberg, 2021); [$] FC: fold change in normalized abundance between
568 virus (V) and no-virus (NV) treatments.

569 **Figure legends.**

570 **Figure 1.** Accumulation of tomato spotted wilt virus (TSWV) proteins in *Frankliniella occidentalis* larval
571 guts. One-way analysis of variance was performed for each protein to determine the effect of larval stage
572 on $\log_2$-transformed, normalized abundance of TSWV proteins detected in the quantitative proteomics
573 dataset: RNA-dependent RNA polymerase (RdRp), two non-structural proteins (NSm and NSs),
574 glycoprotein precursor (GN_GC), and nucleocapsid protein (N). Error bar = standard error of the mean; ns
575 = no significant difference. 3-L1 = first instar larvae, three hours after a 24-hour exposure time on TSWV-
576 infected plant tissue; 48-L2 = second instar larvae ensuing from the 3-L1 cohort, 48 hours after removal
577 from infected plant tissue.

578 **Figure 2.** Differentially abundant proteins in *Frankliniella occidentalis* larval guts after exposure and
579 infection by tomato spotted wilt virus (vDAPs). (A) Volcano plot showcasing the distribution of gut
580 proteins by magnitude of change in normalized abundance of protein between virus (V) and no-virus (NV)
581 conditions and level of significance of that change; proteins with a p-value < 0.05 and fold change ≥ 2 were
582 identified as vDAPs. 3-L1 = first instar larvae, three hours after a 24-hour exposure time to plant tissue of
583 the two conditions (V, NV); 48-L2 = second instar larvae ensuing from the 3-L1 cohort, 48 hours after
584 removal from plant tissue. (B) Venn diagrams showing the numbers of up- and down-regulated vDAPs that
585 are either shared or unique between the two larval stages. The values in parentheses indicate the total
586 number of up- or down-regulated vDAPs in each larval stage. (C) Magnitude and direction of fold changes
587 for vDAPs in common between larval stages.

588 **Figure 3.** Fold change and gene ontology enrichment analysis of differentially abundant proteins in
589 *Frankliniella occidentalis* larval guts after tomato spotted wilt virus exposure (V) and infection compared
590 to the non-exposed (NV) condition (ie., vDAPs = 324 non-redundant proteins across the two larval stages);
591 3-L1 = first instar larvae, three hours after a 24-hour exposure time to plant tissue of the two conditions (V,
592 NV); 48-L2 = second instar larvae ensuing from the 3-L1 cohort, 48 hours after removal from plant tissue.

593 Seventy-nine percent of the vDAP dataset mapped to the *D. melanogaster* (Dm) proteome provided by the
594 program. Enriched gene ontology (GO) terms in the biological process category are displayed, excluding
595 obsolete terms using Revigo web tool; vDAPs with extreme fold change values within each stage and GO
596 term are labeled with Dm ortholog notations: FBXO11 = F-box only protein 11; Cyfip = Cytoplasmic
597 FMR1-interacting protein; Syn = Synapsin-1; alphaTub85E = Tubulin alpha-2 chain; Hsl = Hormone-
598 sensitive lipase; ValRS = Valyl-tRNA synthetase, isoform C; Mcm2 = DNA replication licensing factor
599 Mcm2; PIG-O = Phosphatidylinositol glycan anchor biosynthesis class O; pyx = Pyrexia; Cdc45 = Cell
600 division cycle 45; dpa = Disc proliferation abnormal; verm = Vermiform; CG6013 = uncharacterized
601 protein; CG14120 = uncharacterized protein; IntS1 = Integrator complex subunit 1.

602

603 **Figure 4.** Weighted gene co-expression network analysis (WGCNA) identifies clusters of co-expressed
604 larval gut proteins of *Frankliniella occidentalis.* A) The dendrogram illustrates intermodular relationships,
605 with similar modules grouped together under the same meta-modules (MM); shown as branches on the
606 eigengene dendrogram. Asterisks highlight modules that include sets of differentially abundant proteins in
607 response to tomato spotted wilt virus exposure and infection (vDAPs). B) Module-trait relationships
608 demonstrate significant correlations (*p-value* < 0.05) between modules (clusters of co-expressed proteins,
609 represented as colored blocks on the left side of the column) and the external trait of tomato spotted wilt
610 virus (TSWV) infection. WGCNA analysis was carried out using $\log_2$-transformed, normalized abundance
611 values of all gut-expressed proteins, using samples from both virus-exposed (V) and non-exposed (NV)
612 conditions with four biological replicates. Asterisks denote modules that exhibit a significant association
613 with the external trait of TSWV infection.

614

615 **Figure 5.** Intramodular network analysis of protein co-expression modules significantly correlated with the
616 TSWV condition (see Figure 3B, darkgreen and darkgrey modules). Module membership (kME, correlation
617 of a node to a module eigengene) and intramodular connectivity (kIN, sum of connection weights between

618 a node and all its network neighbors) are plotted for all co-expressed proteins in the (A) darkgreen and (C)
619 darkgrey modules. Pearson's correlation coefficients (r) were calculated on the matrix of kME and kIN
620 values for all proteins in each module. Proteins that ranked within the top 10% in both kME and kIN were
621 considered candidate hub proteins (labeled data points). Intramodular relationships are visualized between
622 co-expressed proteins in the (B) darkgreen and (D) darkgrey module networks. Proteins enclosed by the
623 rounded square boxes represent tomato spotted wilt virus-modulated differentially abundant proteins
624 (vDAPs) *Frankliniella occidentalis* larval guts. Hub proteins in each network are depicted as red
625 rhombuses. Proteins shared between the 3-L1 and 48-L2 developmental stages, as well as those unique to
626 each stage, are indicated by triangle, circle, and square shapes, respectively. For improved network
627 visualization, a weight cutoff of ≥ 0.25 and ≥ 0.20 was applied in the darkgreen and darkgrey modules,
628 respectively. Grey lines show connections between co-expressed proteins, while pink lines indicate hub-
629 protein interconnections. 3-L1 = first instar larvae, three hours after a 24-hour exposure time to plant tissue;
630 48-L2 = second instar larvae ensuing from the 3-L1 cohort, 48 hours after removal from plant tissue.

631 **Figure 6.** Correlations between the abundance of *Frankliniella occidentalis* larval gut proteins and their
632 cognate transcripts for (A) first instar larvae, 3 hours after a 24-hour exposure time on healthy plant tissue
633 (NV 3-L1); (B) first instar larvae, 3 hours after a 24-hour exposure time on TSWV-infected plant tissue (V
634 3-L1); (C) second instar larvae ensuing from the NV 3-L1 cohort, 48 hours after removal of plant tissue
635 (NV 48-L2); and (D) second instar larvae ensuing from the V 3-L1 cohort, 48 hours after removal of
636 infected plant tissue (V 48-L2). Pearson's correlation and linear regression analyses were performed on
637 $\log_2$-transformed normalized abundances values for proteins and their cognate transcript. Blue- and green-
638 colored data points indicate TSWV-modulated, differentially-abundant proteins (vDAPs). Gray and
639 blue/green lines depict best-fit regression lines for the indicated subsets of proteins.

640 **Figure 7.** Associations between larval gut proteins and their cognate transcripts in *Frankliniella*
641 *occidentalis* for the nine network-modules of co-expressed proteins. Spearman's rank correlation
642 coefficients (ρ) were calculated on $\log_2$-transformed, normalized abundance of proteins and transcripts each

643 larval stage - virus condition combination for each of the network modules. The number within parentheses
644 () indicates the number of proteins within each module. V/NV = virus-exposed (and infected)/non-exposed;
645 3-L1 = first instar larvae, three hours after a 24-hour exposure to the condition (V or NV); 48-L2 = second
646 instar larvae ensuing from the 3-L1 cohort, 48 hours post exposure to the condition.

647 **REFERENCES**

648 Abekhoukh, S., Sahin, H.B., Grossi, M., Zongaro, S., Maurin, T., Madrigal, I., Kazue-Sugioka, D., Raas-
649 Rothschild, A., Doulazmi, M., Carrera, P., Stachon, A., Scherer, S., Drula Do Nascimento, M.R.,
650 Trembleau, A., Arroyo, I., Szatmari, P., Smith, I.M., Mila, M., Smith, A.C., Giangrande, A., Caillé,
651 I., Bardoni, B., 2017. New insights into the regulatory function of CYFIP1 in the context of WAVE-
652 and FMRP-containing complexes. Dis Model Mech 10, 463. https://doi.org/10.1242/DMM.025809

653 Altaf-Ul-Amin, M., Afendi, F.M., Kiboi, S.K., Kanaya, S., 2014. Systems biology in the context of big
654 data and networks. Biomed Res Int 2014. https://doi.org/10.1155/2014/428570

655 Badillo-Vargas, I.E., Chen, Y., Martin, K.M., Rotenberg, D., Whitfield, A.E., 2019. Discovery of novel
656 thrips vector proteins that bind to the plant bunyavirus tomato spotted wilt virus. J Virol 93.
657 https://doi.org/10.1128/jvi.00699-19

658 Badillo-Vargas, I.E., Rotenberg, D., Schneweis, D.J., Hiromasa, Y., Tomich, J.M., Whitfield, A.E., 2012.
659 Proteomic analysis of *Frankliniella occidentalis* and differentially expressed proteins in response to
660 *Tomato spotted wilt virus* infection. J Virol 86, 8793–8809. https://doi.org/10.1128/jvi.00285-12

661 Ben-Ze'ev, A., Farmer, S.R., Penman, S., 1979. Mechanisms of regulating tubulin synthesis in cultured
662 mammalian cells. Cell 17, 319–325. https://doi.org/10.1016/0092-8674(79)90157-0

663 Brault, V., Tanguy, S., Reinbold, C., Le Trionnaire, G., Arneodo, J., Jaubert-Possamai, S., Guernec, G.,
664 Tagu, D., 2010. Transcriptomic analysis of intestinal genes following acquisition of pea enation

665 mosaic virus by the pea aphid *Acyrthosiphon pisum*. Journal of General Virology 91, 802–808.
666 https://doi.org/10.1099/vir.0.012856-0

667 Chiapello, M., Bosco, L., Ciuffo, M., Ottati, S., Salem, N, Rosa, C., Tavella, L., Turina, M. (2021).
668 Complexity and local specificity of the virome associated with tospovirus-transmitting thrips species.
669 *J Virol.* 95(21):e0059721. doi: 10.1128/JVI.00597-21.

670 De Assis Filho, F.M., Naidu, R.A., Deom, C.M., Sherwood, J.L., 2002. Dynamics of *Tomato spotted wilt*
671 *virus* replication in the alimentary canal of two thrips species. Phytopathology 92, 729–733.
672 https://doi.org/10.1094/PHYTO.2002.92.7.729

673 Deng, Z., Fan, T., Xiao, C., Tian, H., Zheng, Y., Li, C., He, J., 2024. TGF-β signaling in health, disease
674 and therapeutics. Signal Transduct Target Ther 9, 61. https://doi.org/10.1038/S41392-024-01764-W

675 Deribe, Y.L., Pawson, T., Dikic, I., 2010. Post-translational modifications in signal integration. Nat Struct
676 Mol Biol 17, 666–672. https://doi.org/10.1038/NSMB.1842

677 Desai, A., Mitchison, T.J., 1997. Microtubule polymerization dynamics. Annu Rev Cell Dev Biol 13, 83–
678 117. https://doi.org/10.1146/ANNUREV.CELLBIO.13.1.83

679 Dietzgen, R.G., Mann, K.S., Johnson, K.N., 2016. Plant virus-insect vector interactions: Current and
680 potential future research directions. Viruses 8, 1–21. https://doi.org/10.3390/v8110303

681 Du, Y., Clair, G.C., Al Alam, D., Danopoulos, S., Schnell, D., Kitzmiller, J.A., Misra, R.S., Bhattacharya,
682 S., Warburton, D., Mariani, T.J., Pryhuber, G.S., Whitsett, J.A., Ansong, C., Xu, Y., 2019.
683 Integration of transcriptomic and proteomic data identifies biological functions in cell populations
684 from human infant lung. Am J Physiol Lung Cell Mol Physiol 317, L347.
685 https://doi.org/10.1152/AJPLUNG.00475.2018

686 Elliott, R.M., Schmaljohn, C.S., 2013. The bunyaviridae, 6th ed. Wolters Kluwer.

687 Gasic, I., Boswell, S.A., Mitchison, T.J., 2019. Tubulin mRNA stability is sensitive to change in
688 microtubule dynamics caused by multiple physiological and toxic cues. PLoS Biol 17.
689 https://doi.org/10.1371/JOURNAL.PBIO.3000225

690 Geng, L., Qian, L.X., Shao, R.X., Liu, Y.Q., Liu, S.S., Wang, X.W., 2018. Transcriptome profiling of
691 whitefly guts in response to *Tomato yellow leaf curl virus* infection. Virol J 15, 1–12.
692 https://doi.org/10.1186/s12985-018-0926-6

693 Ghosh, S., Ghanim, M., 2021. Factors determining transmission of persistent viruses by *Bemisia tabaci*
694 and emergence of new virus-vector relationships. Viruses. https://doi.org/10.3390/v13091808

695 Gong, Y., Li, Y., Liu, D., Jiang, L., Liang, H., Wu, Y., Wang, F., Yang, J., 2023. Analysis of lysine
696 acetylation in tomato spot wilt virus infection in Nicotiana benthamiana. Front Microbiol 14.
697 https://doi.org/10.3389/FMICB.2023.1046163

698 Götz, S., García-Gómez, J.M., Terol, J., Williams, T.D., Nagaraj, S.H., Nueda, M.J., Robles, M., Talón,
699 M., Dopazo, J., Conesa, A., 2008. High-throughput functional annotation and data mining with the
700 Blast2GO suite. Nucleic Acids Res 36, 3420–3435. https://doi.org/10.1093/NAR/GKN176

701 Gygi, S.P., Rochon, Y., Franza, B.R., Aebersold, R., 1999. Correlation between Protein and mRNA
702 Abundance in Yeast. Mol Cell Biol 19, 1720–1730.
703 https://doi.org/10.1128/MCB.19.3.1720/ASSET/DBC7033A-DCFA-438A-BA94-
704 F79C524792FD/ASSETS/GRAPHIC/MB0391587007.JPEG

705 Han, J., Rotenberg, D., 2021. Integration of transcriptomics and network analysis reveals co-expressed
706 genes in *Frankliniella occidentalis* larval guts that respond to tomato spotted wilt virus infection.
707 BMC Genomics 22, 1–17. https://doi.org/10.1186/s12864-021-08100-4

708 Heck, M., 2018. Insect transmission of plant pathogens: a systems biology perspective. mSystems 3.
709 https://doi.org/10.1128/msystems.00168-17

710 Hu, Z., Mellor, J., Wu, J., DeLisi, C., 2004. VisANT: An online visualization and analysis tool for
711 biological interaction data. BMC Bioinformatics 5, 17. https://doi.org/10.1186/1471-2105-5-17

712 Kim, M.S., Zhong, J., Pandey, A., 2016. Common errors in mass spectrometry-based analysis of post-
713 translational modifications. Proteomics 16, 700. https://doi.org/10.1002/PMIC.201500355

714 Langfelder, P., Horvath, S., 2008. WGCNA: An R package for weighted correlation network analysis.
715 BMC Bioinformatics 9, 559. https://doi.org/10.1186/1471-2105-9-559

716 Lee, Y.S., Pressman, S., Andress, A.P., Kim, K., White, J.L., Cassidy, J.J., Li, X., Lubell, K., Lim, D.H.,
717 Cho, I.S., Nakahara, K., Preall, J.B., Bellare, P., Sontheimer, E.J., Carthew, R.W., 2009. Silencing
718 by small RNAs is linked to endosomal trafficking. Nat Cell Biol 11, 1150–1156.
719 https://doi.org/10.1038/NCB1930

720 Li, Y., Chen, D., Hu, J., Zhang, K., Kang, L., Chen, Y., Huang, L., Zhang, L., Xiang, Y., Song, Q., Liu,
721 F., 2020. The α-tubulin of Laodelphax striatellus mediates the passage of rice stripe virus (RSV) and
722 enhances horizontal transmission. PLoS Pathog 16, e1008710.
723 https://doi.org/10.1371/JOURNAL.PPAT.1008710

724 Liu, Y., Beyer, A., Aebersold, R., 2016. On the Dependency of Cellular Protein Levels on mRNA
725 Abundance. Cell 165, 535–550. https://doi.org/10.1016/J.CELL.2016.03.014

726 Massagué, J., 2012. TGFβ signalling in context. Nature Reviews Molecular Cell Biology 2012 13:10 13,
727 616–630. https://doi.org/10.1038/nrm3434

728 Mata, J., Marguerat, S., Bähler, J., 2005. Post-transcriptional control of gene expression: a genome-wide
729 perspective. Trends Biochem Sci 30, 506–514. https://doi.org/10.1016/J.TIBS.2005.07.005

730 McCarthy, J.E.G., 1998. Posttranscriptional control of gene expression in yeast. Microbiology and
731 Molecular Biology Reviews 62, 1492–1553. https://doi.org/10.1128/MMBR.62.4.1492-

732 1553.1998/ASSET/036685BD-8E5F-48E6-A976-
733 5F0A0B53674E/ASSETS/GRAPHIC/MR0480047018.JPEG

734 Montero-Astúa, M., Stafford, C., Badillo-Vargas, I., Rotenberg, D., Ullman, D., Whitfield, A.E., 2016a.
735 Tospovirus–thrips biology, in: Brown, J.K. (Ed.), Vector-Mediated Transmission of Plant
736 Pathogens. The American Phytopathological Society, pp. 289–308.
737 https://doi.org/10.1094/9780890545355.020

738 Montero-Astúa, M., Ullman, D.E., Whitfield, A.E., 2016b. Salivary gland morphology, tissue tropism and
739 the progression of tospovirus infection in *Frankliniella occidentalis*. Virology 493, 39–51.
740 https://doi.org/10.1016/j.virol.2016.03.003

741 Moritz, G., Kumm, S., Mound, L., 2004. Tospovirus transmission depends on thrips ontogeny. Virus Res
742 100, 143–149. https://doi.org/10.1016/j.virusres.2003.12.022

743 Naghavi, M.H., Walsh, D., 2017. Microtubule regulation and function during virus infection. J Virol 91.
744 https://doi.org/10.1128/JVI.00538-17

745 Napoli, I., Mercaldo, V., Boyl, P.P., Eleuteri, B., Zalfa, F., De Rubeis, S., Di Marino, D., Mohr, E.,
746 Massimi, M., Falconi, M., Witke, W., Costa-Mattioli, M., Sonenberg, N., Achsel, T., Bagni, C.,
747 2008. The fragile X syndrome protein represses activity-dependent translation through CYFIP1, a
748 new 4E-BP. Cell 134, 1042–1054. https://doi.org/10.1016/J.CELL.2008.07.031

749 Ohi, R., Strothman, C., Zanic, M., 2021. Impact of the "tubulin economy" on the formation and function
750 of the microtubule cytoskeleton. Curr Opin Cell Biol 68, 81–89.
751 https://doi.org/10.1016/J.CEB.2020.09.005

752 Ohnishi, J., Knight, L.M., Hosokawa, D., Fujisawa, I., Tsuda, S., 2001. Replication of *Tomato spotted*
753 *wilt virus* after ingestion by adult *Thrips setosus* is restricted to midgut epithelial cells.
754 Phytopathology 91, 1149–1155. https://doi.org/10.1094/PHYTO.2001.91.12.1149

755 Payne, S.H., 2015. The utility of protein and mRNA correlation. Trends Biochem Sci 40, 1–3.
756 https://doi.org/10.1016/J.TIBS.2014.10.010

757 Pham, N.T.K., Trinh, Q.D., Takada, K., Takano, C., Sasano, M., Okitsu, S., Ushijima, H., Komine-
758 Aizawa, S., Hayakawa, S., 2021. The Epithelial-to-Mesenchymal Transition-Like Process Induced
759 by TGF-β1 Enhances Rubella Virus Binding and Infection in A549 Cells via the Smad Pathway.
760 Microorganisms 9, 662. https://doi.org/10.3390/MICROORGANISMS9030662

761 Pradet-Balade, B., Boulmé, F., Beug, H., Müllner, E.W., Garcia-Sanz, J.A., 2001. Translation control:
762 bridging the gap between genomics and proteomics? Trends Biochem Sci 26, 225–229.
763 https://doi.org/10.1016/S0968-0004(00)01776-X

764 Rajarapu, S.P., Ben-Mahmoud, S., Benoit, J.B., Ullman, D.E., Whitfield, A.E., Rotenberg, D., 2022. Sex-
765 biased proteomic response to tomato spotted wilt virus infection of the salivary glands of
766 *Frankliniella occidentalis*, the western flower thrips. Insect Biochem Mol Biol 149, 103843.
767 https://doi.org/10.1016/J.IBMB.2022.103843

768 Richmond, G.S., Smith, T.K., 2011. Phospholipases A1. International Journal of Molecular Sciences
769 2011, Vol. 12, Pages 588-612 12, 588–612. https://doi.org/10.3390/IJMS12010588

770 Rotenberg, D., Gibbs, R.A., Worley, K.C., Murali, S.C., Lee, S.L., Muzny, D.M., Hughes, D.S.T., Chao,
771 H., Dinh, H., Doddapaneni, H., Qu, J., Dugan-Perez, S., Han, Y., Richards, S., 2019a. *Frankliniella*
772 *occidentalis* genome assembly v1.0. Ag Data Commons (Database) [WWW Document]. URL
773 https://doi.org/10.15482/USDA.ADC/1503960

774 Rotenberg, D., Jacobson, A.L., Schneweis, D.J., Whitfield, A.E., 2015. Thrips transmission of
775 tospoviruses. Curr Opin Virol 15, 80–89. https://doi.org/10.1016/j.coviro.2015.08.003

776 Rotenberg, D., Robertson, H.M., Oliver, J.E., Benoit, J.B., Snoeck, S., Baumann, A.A., Mahmoud, S.
777 Ben, Veenstra, J.A., Jacobs, C.G.C., Park, Y., Panfilio, K.A., Widana Gamage, S.M.K., Ahn, S.-J.,

778 Vargas Jentzsch, I.M., Jennings, E.C., Szuter, E.M., Christiaens, O., Scanlan, J., Taning, C.N.T.,
779 Martynov, A., Bejerman, N.E., Nair, A., Jones, J.W., Friedrich, M., van der Zee, M., Dearden, P.,
780 Minakuchi, C., Armisén, D., Schneweis, D.J., Melo, F.L., Poelchau, M., Dermauw, W., Hughes,
781 D.S.T., Richards, S., Didion, E.M., Holmes, C.J., Rosendale, A.J., Rosselot, A., Dolan, A.,
782 Whitfield, A.E., Ullman, D.E., Dietzgen, R.G., Smagghe, G., Van Leeuwen, T., Warren, J.H.,
783 2019b. *Frankliniella occidentalis* Official Gene Set OGSv1.0. Ag Data Commons (Database)
784 [WWW Document]. URL https://doi.org/10.15482/USDA.ADC/1504029

785 Rotenberg, D., Whitfield, A.E., 2018. Molecular interactions between tospoviruses and thrips vectors.
786 Curr Opin Virol 33, 191–197. https://doi.org/10.1016/j.coviro.2018.11.007

787 Schneweis, D.J., Whitfield, A.E., Rotenberg, D., 2017. Thrips developmental stage-specific transcriptome
788 response to tomato spotted wilt virus during the virus infection cycle in *Frankliniella occidentalis*,
789 the primary vector. Virology 500, 226–237. https://doi.org/10.1016/j.virol.2016.10.009

790 Shi, J., Zhou, J., Jiang, F., Li, Z., Zhu, S., 2023. The effects of the E3 ubiquitin-protein ligase UBR7 of
791 *Frankliniella occidentalis* on the ability of insects to acquire and transmit TSWV. PeerJ 11.
792 https://doi.org/10.7717/PEERJ.15385

793 Silva, C.P., Silva, J.R., Vasconcelos, F.F., Petretski, M.D.A., DaMatta, R.A., Ribeiro, A.F., Terra, W.R.,
794 2004. Occurrence of midgut perimicrovillar membranes in paraneopteran insect orders with
795 comments on their function and evolutionary significance. Arthropod Struct Dev 33, 139–148.
796 https://doi.org/10.1016/j.asd.2003.12.002

797 Srivastava, H., Lippincott, M.J., Currie, J., Canfield, R., Lam, M.P.Y., Lau, E., 2022. Protein prediction
798 models support widespread post-transcriptional regulation of protein abundance by interacting
799 partners. PLoS Comput Biol 18. https://doi.org/10.1371/JOURNAL.PCBI.1010702

800 Stafford-Banks, C.A., Rotenberg, D., Johnson, B.R., Whitfield, A.E., Ullman, D.E., 2014. Analysis of the
801 salivary gland transcriptome of *Frankliniella occidentalis*. PLoS One 9, e94447.
802 https://doi.org/10.1371/journal.pone.0094447

803 Sunnerhagen, P., 2007. Cytoplasmatic post-transcriptional regulation and intracellular signalling. Mol
804 Genet Genomics 277, 341–355. https://doi.org/10.1007/S00438-007-0221-5

805 Szklarczyk, D., Kirsch, R., Koutrouli, M., Nastou, K., Mehryary, F., Hachilif, R., Gable, A.L., Fang, T.,
806 Doncheva, N.T., Pyysalo, S., Bork, P., Jensen, L.J., Von Mering, C., 2023. The STRING database in
807 2023: protein-protein association networks and functional enrichment analyses for any sequenced
808 genome of interest. Nucleic Acids Res 51, D638–D646. https://doi.org/10.1093/NAR/GKAC1000

809 Tasaki, S., Xu, J., Avey, D.R., Johnson, L., Petyuk, V.A., Dawe, R.J., Bennett, D.A., Wang, Y., Gaiteri,
810 C., 2022. Inferring protein expression changes from mRNA in Alzheimer's dementia using deep
811 neural networks. Nat Commun 13. https://doi.org/10.1038/S41467-022-28280-1

812 Trinh, Q.D., Pham, N.T.K., Takada, K., Takano, C., Komine-Aizawa, S., Hayakawa, S., 2022. TGF-β1
813 promotes Zika virus infection in immortalized human first-trimester trophoblasts via the Smad
814 pathway. Cells 11, 3026. https://doi.org/10.3390/CELLS11193026/S1

815 Ullman, D.E., 1992. A midgut barrier to tomato spotted wilt virus acquisition by adult western flower
816 thrips. Phytopathology 82, 1333. https://doi.org/10.1094/phyto-82-1333

817 Ullman, D.E., German, T.L., Sherwood, J.L., Westcot, D.M., Cantone, F.A., 1993. Tospovirus replication
818 in insect vector cells: immunocytochemical evidence that the nonstructural protein encoded by the S
819 RNA of tomato spotted wilt tospovirus is present in thrips vector cells. Phytopathology 83, 456.
820 https://doi.org/10.1094/phyto-83-456

821 Ullman, D.E., Westcot, D.M., Chenault, K.D., Sherwood, J.L., German, T.L., Bandla, M.D., Cantone,
822 F.A., Duer, H.L., 1995. Compartmentalization, intracellular transport, and autophagy of tomato

823 spotted wilt tospovirus proteins in infected thrips cells. Phytopathology 85, 644–654.
824 https://doi.org/10.1094/Phyto-85-644

825 Van De Wetering, F., Goldbach, R., Peters, D., 1996. Tomato spotted wilt tospovirus ingestion by first
826 instar larvae of *Frankliniella occidentalis* is a prerequisite for transmission. Phytopathology 86,
827 900–905. https://doi.org/10.1094/phyto-86-900

828 Vogel, C., Marcotte, E.M., 2012. Insights into the regulation of protein abundance from proteomic and
829 transcriptomic analyses. Nature Reviews Genetics 2012 13:4 13, 227–232.
830 https://doi.org/10.1038/nrg3185

831 Zhao, B.S., Roundtree, I.A., He, C., 2016. Post-transcriptional gene regulation by mRNA modifications.
832 Nature Reviews Molecular Cell Biology 2016 18:1 18, 31–42. https://doi.org/10.1038/nrm.2016.132

833 Zhao, L., Wang, D., Wang, Q., Rodal, A.A., Zhang, Y.Q., 2013. Drosophila cyfip regulates synaptic
834 development and endocytosis by suppressing filamentous actin assembly. PLoS Genet 9, e1003450.
835 https://doi.org/10.1371/JOURNAL.PGEN.1003450

836 Zhao, W., Lu, L., Yang, P., Cui, N., Kang, L., Cui, F., 2016. Organ-specific transcriptome response of the
837 small brown planthopper toward rice stripe virus. Insect Biochem Mol Biol 70, 60–72.
838 https://doi.org/10.1016/j.ibmb.2015.11.009

839 Zhu, K.Y., Merzendorfer, H., Zhang, W., Zhang, J., Muthukrishnan, S., 2016. Biosynthesis, turnover, and
840 functions of chitin in insects. Annu Rev Entomol 61, 177–196. https://doi.org/10.1146/ANNUREV-
841 ENTO-010715-023933

842

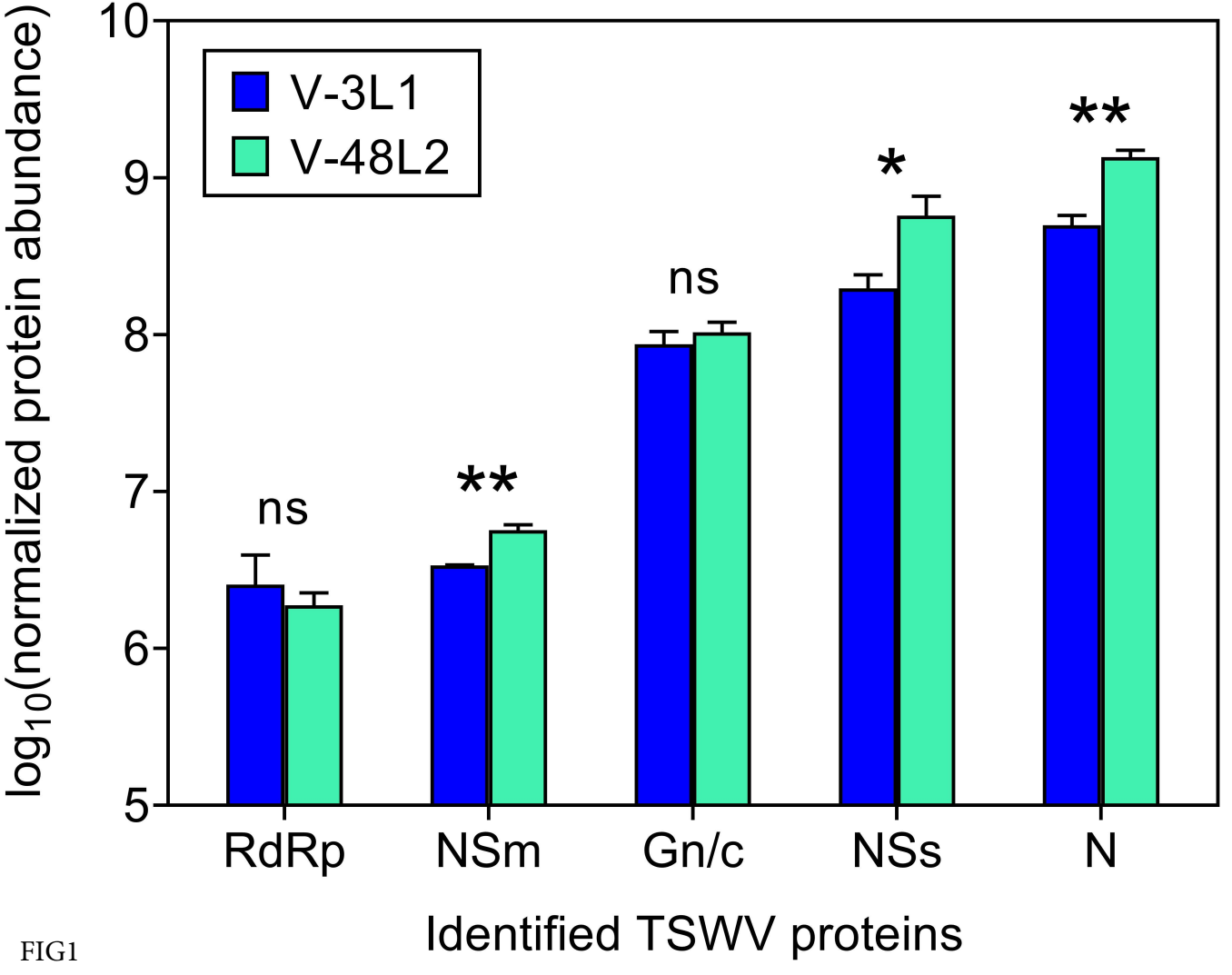
V-3L1
V-48L2
10
9
8
7
6
5
log10(normalized protein abundance)
ns
**
ns
*
**
RdRp
NSm
Gn/c
NSs
N
Identified TSWV proteins

FIG1

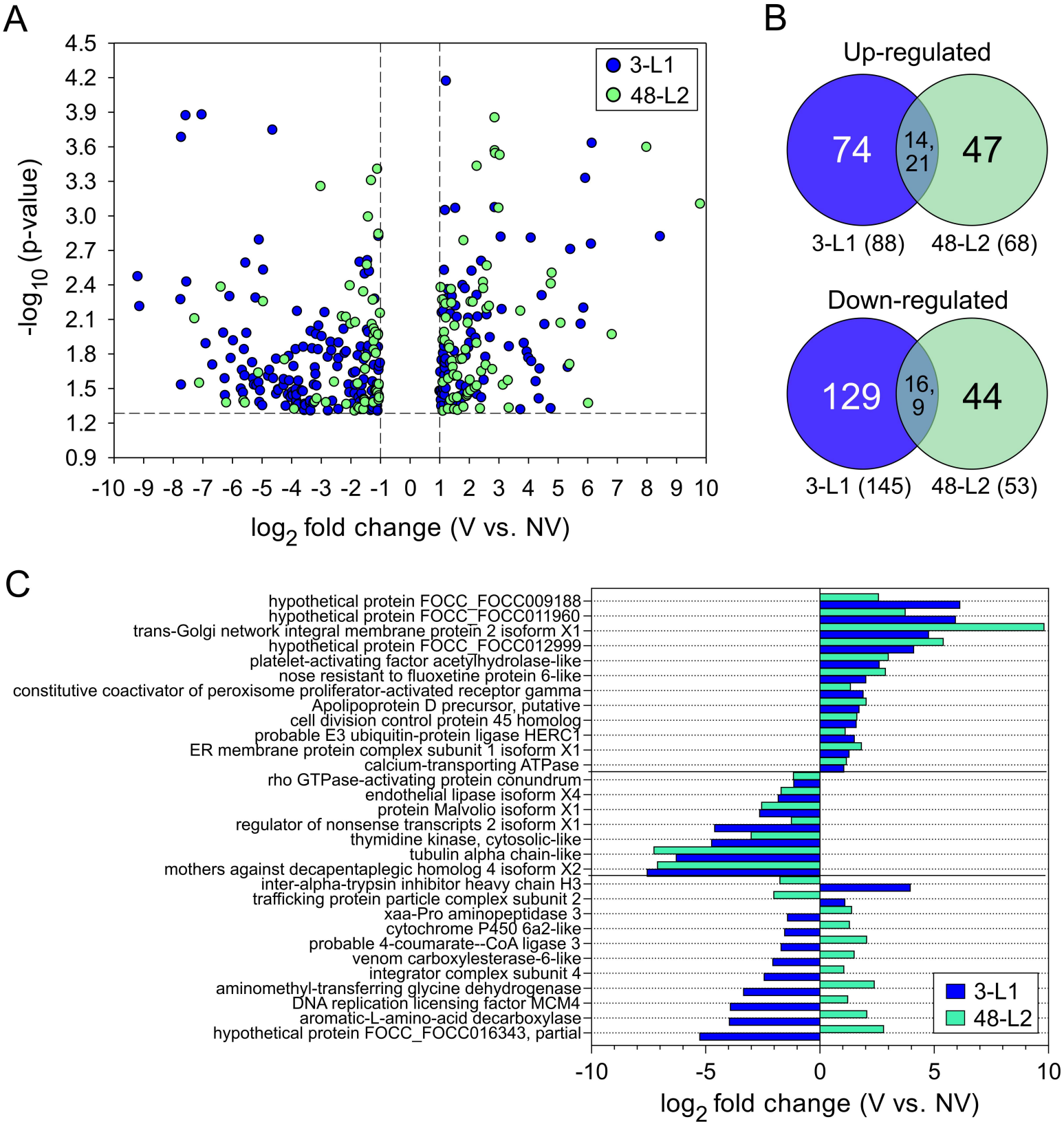
A
3-L1
48-L2
-log10 (p-value)
log2 fold change (V vs. NV)
B
Up-regulated
74
14, 21
47
3-L1 (88)
48-L2 (68)
Down-regulated
129
16, 9
44
3-L1 (145)
48-L2 (53)
C
hypothetical protein FOCC_FOCC009188
hypothetical protein FOCC_FOCC011960
trans-Golgi network integral membrane protein 2 isoform X1
hypothetical protein FOCC_FOCC012999
platelet-activating factor acetylhydrolase-like
nose resistant to fluoxetine protein 6-like
constitutive coactivator of peroxisome proliferator-activated receptor gamma
Apolipoprotein D precursor, putative
cell division control protein 45 homolog
probable E3 ubiquitin-protein ligase HERC1
ER membrane protein complex subunit 1 isoform X1
calcium-transporting ATPase
rho GTPase-activating protein conundrum
endothelial lipase isoform X4
protein Malvolio isoform X1
regulator of nonsense transcripts 2 isoform X1
thymidine kinase, cytosolic-like
tubulin alpha chain-like
mothers against decapentaplegic homolog 4 isoform X2
inter-alpha-trypsin inhibitor heavy chain H3
trafficking protein particle complex subunit 2
xaa-Pro aminopeptidase 3
cytochrome P450 6a2-like
probable 4-coumarate--CoA ligase 3
venom carboxylesterase-6-like
integrator complex subunit 4
aminomethyl-transferring glycine dehydrogenase
DNA replication licensing factor MCM4
aromatic-L-amino-acid decarboxylase
hypothetical protein FOCC_FOCC016343, partial
3-L1
48-L2
log2 fold change (V vs. NV)

FIG2

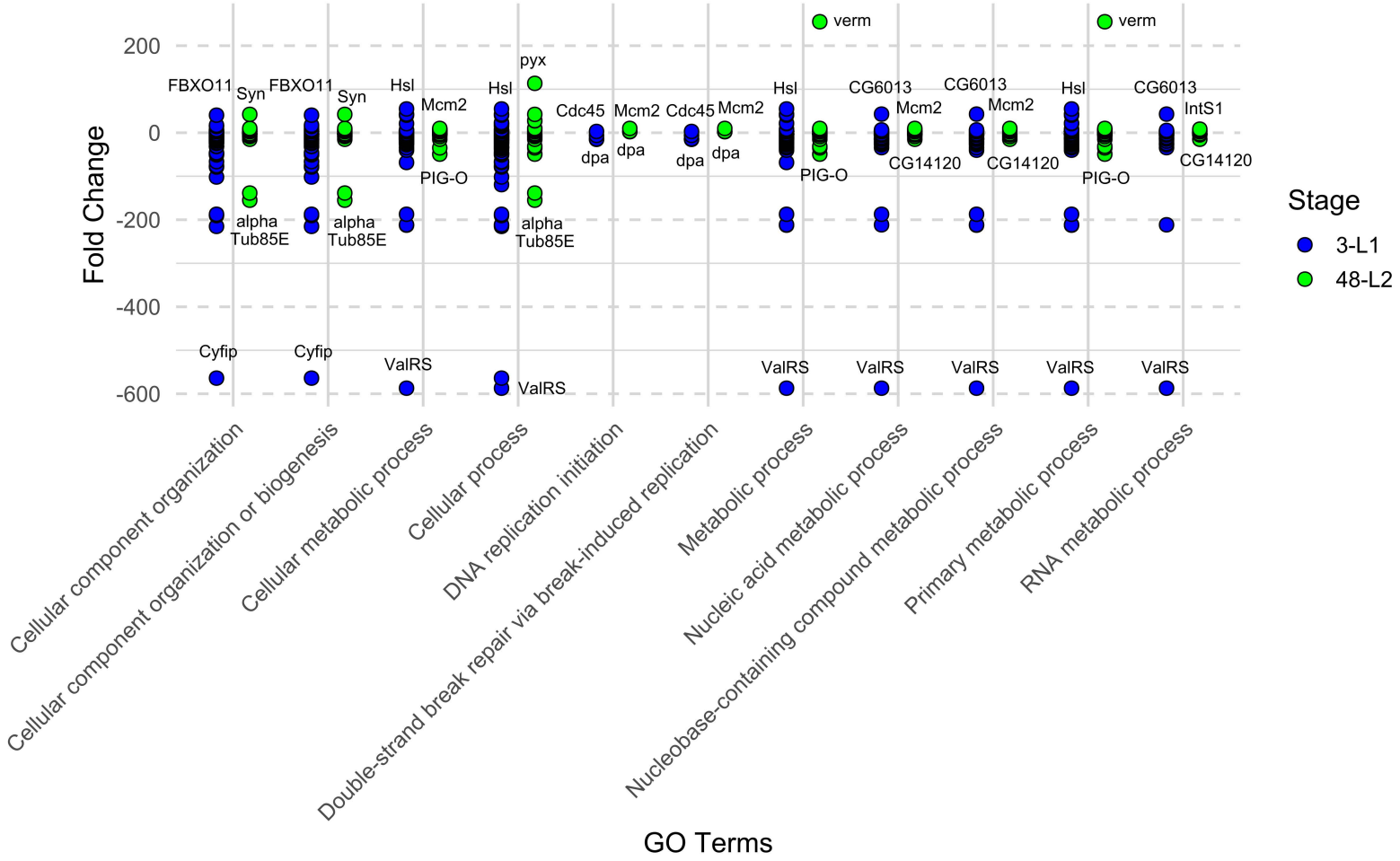
Fold Change
200
0
-200
-400
-600
FBXO11
Syn
alpha Tub85E
Cyfip
Hsl
Mcm2
PIG-O
ValRS
pyx
Cdc45
dpa
verm
CG6013
CG14120
IntS1
Cellular component organization
Cellular component organization or biogenesis
Cellular metabolic process
Cellular process
DNA replication initiation
Double-strand break repair via break-induced replication
Metabolic process
Nucleic acid metabolic process
Nucleobase-containing compound metabolic process
Primary metabolic process
RNA metabolic process
GO Terms
Stage
3-L1
48-L2

FIG3

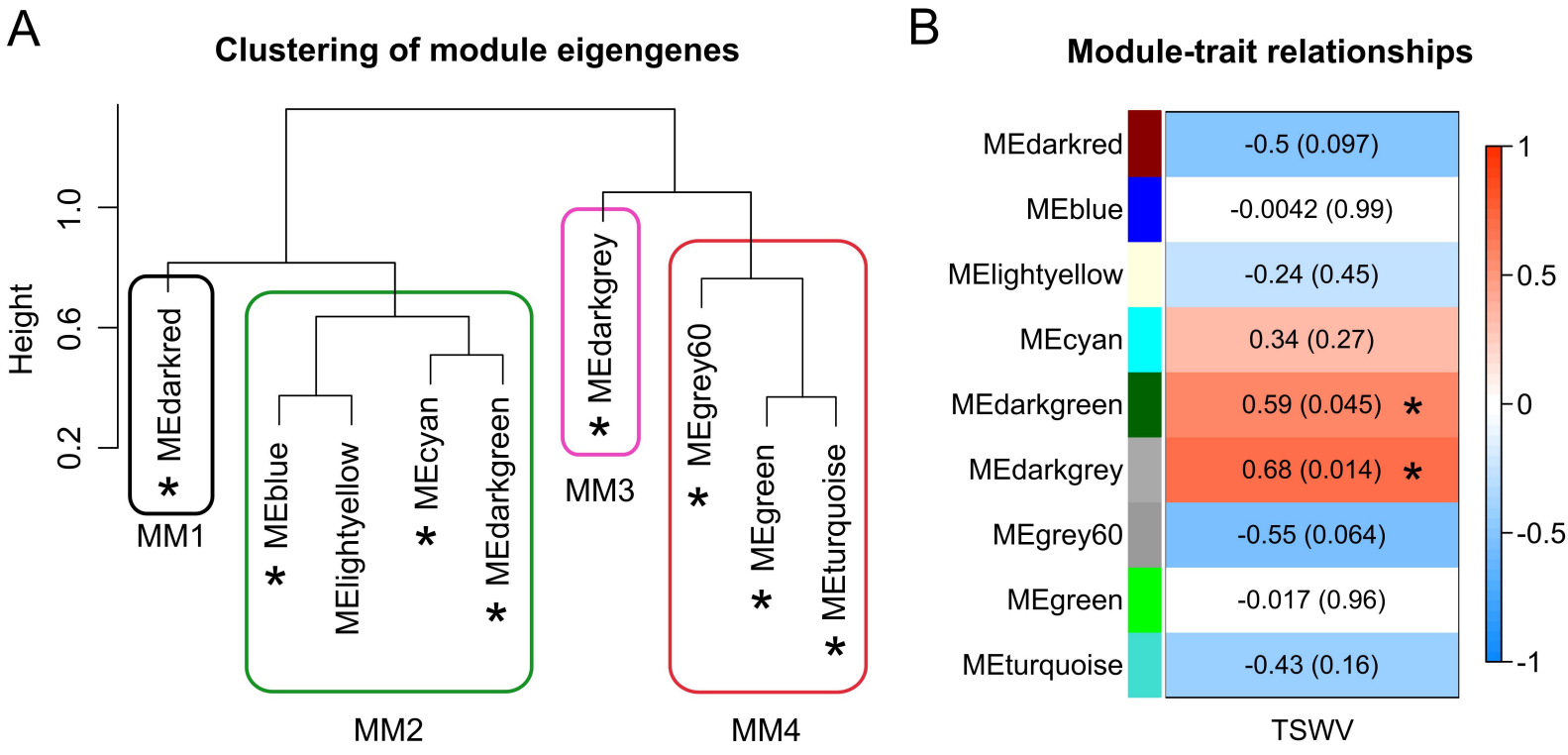
A
Clustering of module eigengenes
Height
1.0
0.6
0.2
* MEdarkred
MM1
* MEblue
MElightyellow
* MEcyan
* MEdarkgreen
MM2
* MEdarkgrey
MM3
* MEgrey60
* MEgreen
* MEturquoise
MM4
B
Module-trait relationships
MEdarkred
MEblue
MElightyellow
MEcyan
MEdarkgreen
MEdarkgrey
MEgrey60
MEgreen
MEturquoise
-0.5 (0.097)
-0.0042 (0.99)
-0.24 (0.45)
0.34 (0.27)
0.59 (0.045) *
0.68 (0.014) *
-0.55 (0.064)
-0.017 (0.96)
-0.43 (0.16)
TSWV
1
0.5
0
-0.5
-1

FIG4

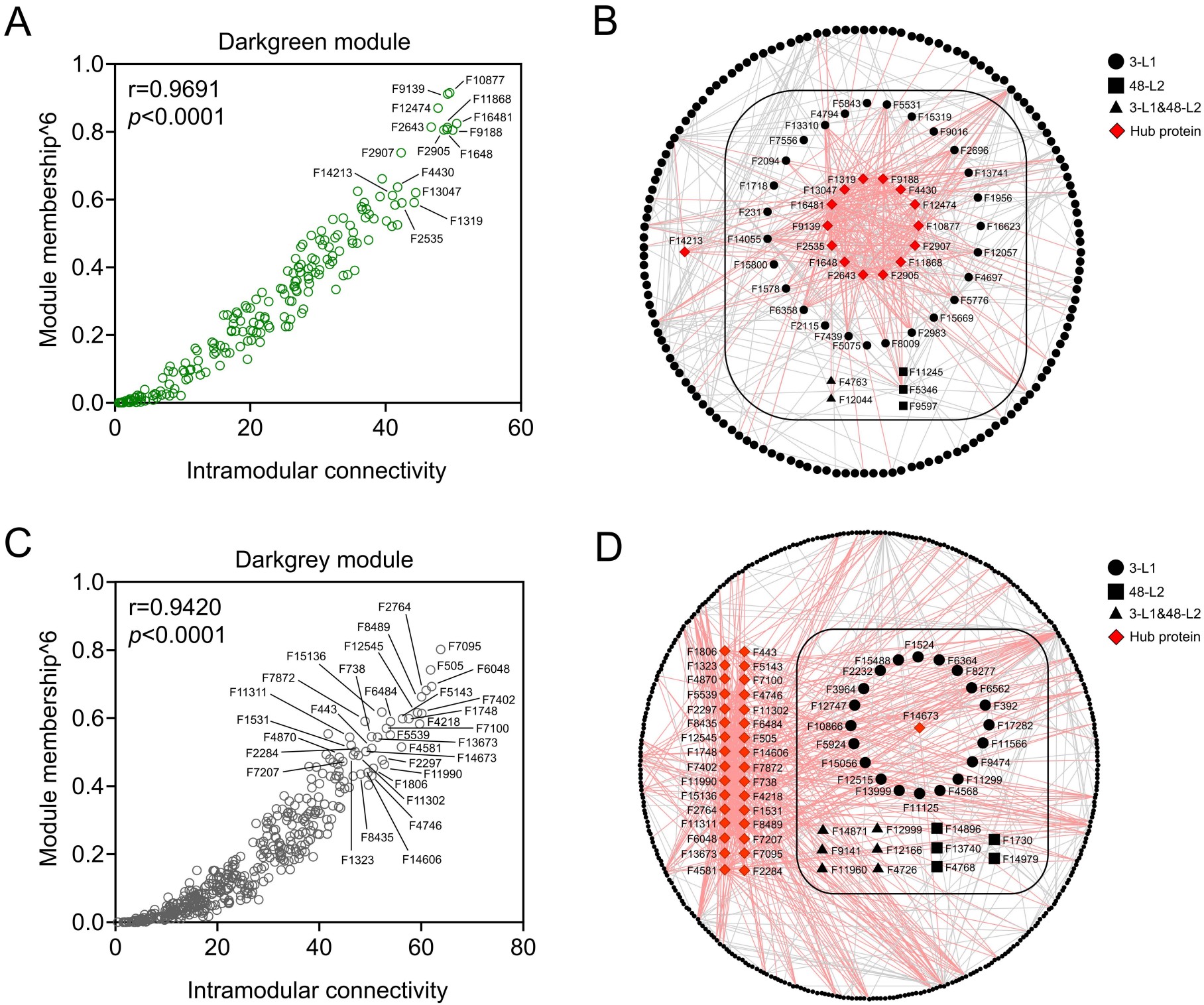
A
Darkgreen module
r=0.9691
p<0.0001
Module membership^6
Intramodular connectivity
F10877
F9139
F11868
F12474
F16481
F2643
F9188
F2907
F2905
F1648
F14213
F4430
F13047
F1319
F2535
B
3-L1
48-L2
3-L1&48-L2
Hub protein
C
Darkgrey module
r=0.9420
p<0.0001
Module membership^6
Intramodular connectivity
F2764
F8489
F12545
F7095
F15136
F505
F6048
F738
F7872
F6484
F5143
F11311
F7402
F443
F1748
F4218
F1531
F7100
F5539
F4870
F13673
F4581
F2284
F14673
F2297
F7207
F11990
F1806
F11302
F4746
F8435
F1323
F14606
D
3-L1
48-L2
3-L1&48-L2
Hub protein

FIG5

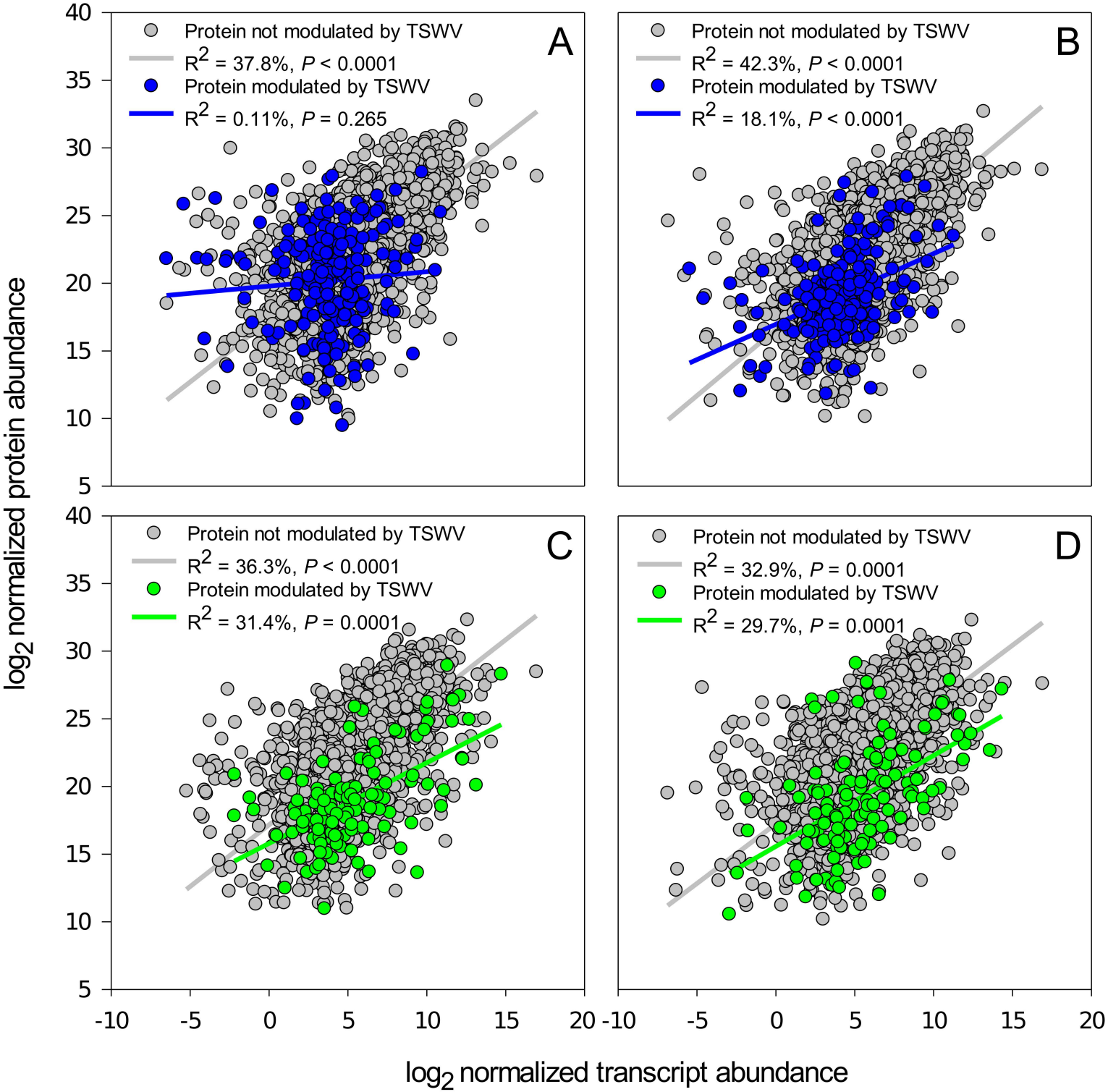
A
Protein not modulated by TSWV
R2 = 37.8%, P < 0.0001
Protein modulated by TSWV
R2 = 0.11%, P = 0.265
B
Protein not modulated by TSWV
R2 = 42.3%, P < 0.0001
Protein modulated by TSWV
R2 = 18.1%, P < 0.0001
C
Protein not modulated by TSWV
R2 = 36.3%, P < 0.0001
Protein modulated by TSWV
R2 = 31.4%, P = 0.0001
D
Protein not modulated by TSWV
R2 = 32.9%, P = 0.0001
Protein modulated by TSWV
R2 = 29.7%, P = 0.0001
log2 normalized protein abundance
log2 normalized transcript abundance
40
35
30
25
20
15
10
5
-10
-5
0
5
10
15
20

FIG6

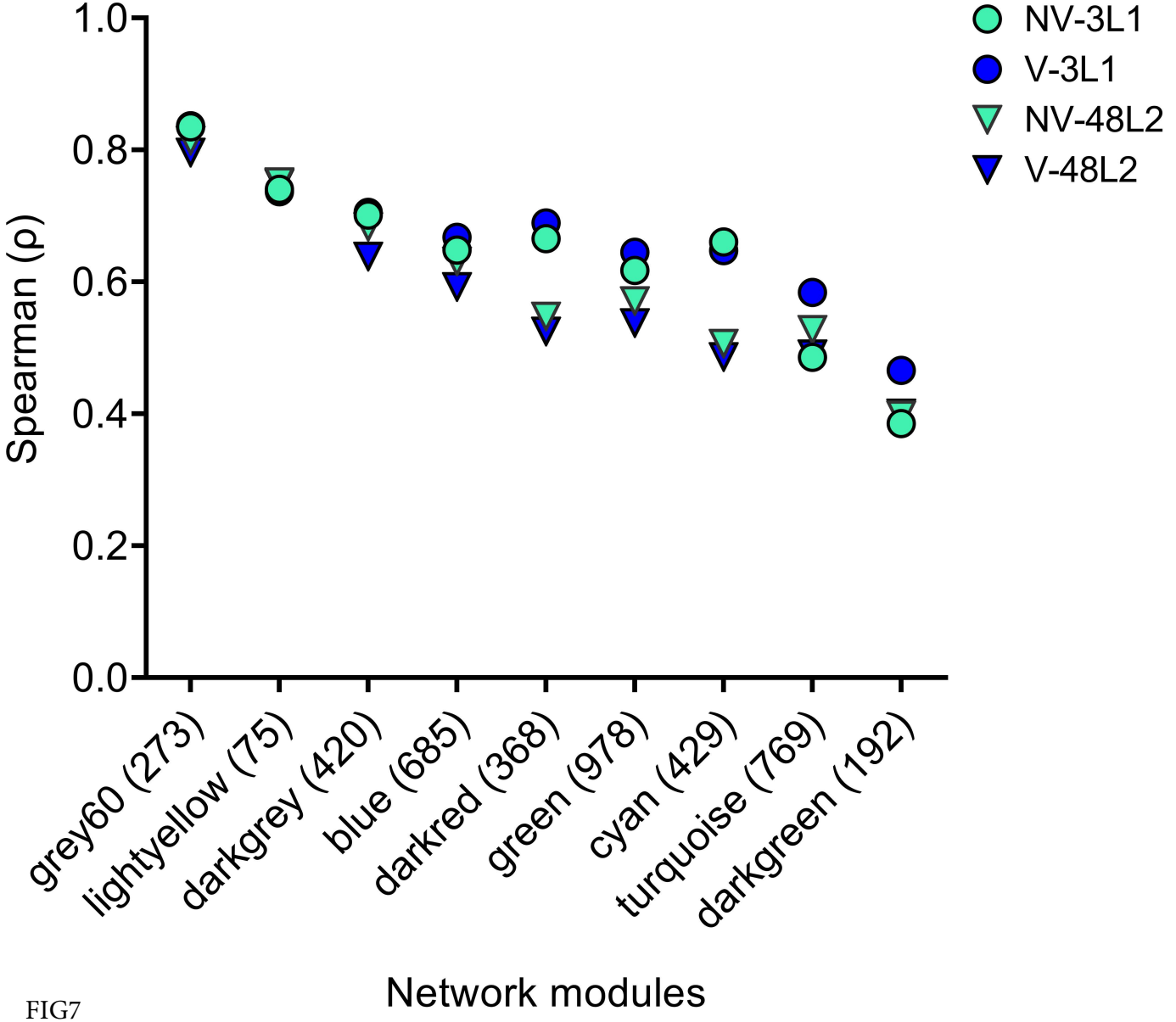
NV-3L1
V-3L1
NV-48L2
V-48L2
Spearman (ρ)
1.0
0.8
0.6
0.4
0.2
0.0
grey60 (273)
lightyellow (75)
darkgrey (420)
blue (685)
darkred (368)
green (978)
cyan (429)
turquoise (769)
darkgreen (192)
Network modules

FIG7